N84-20672

NASA Technical Memorandum 83580

Mechanism of Corrosion of Ni Base Superalloys by Molten Na_2MoO_4 at Elevated Temperatures

Ajaya K. Misra and Carl A. Stearns
Lewis Research Center
Cleveland, Ohio

Prepared for the
Fall Meeting of the Electrochemical Society
Washington, D.C., October 9-14, 1983

NASA

MECHANISM OF CORROSION OF Ni BASE SUPERALLOYS

BY MOLTEN Na_2MoO_4 AT ELEVATED TEMPERATURES

by Ajaya K. Misra* and Carl A. Stearns

National Aeronautics and Space Administration
Lewis Research Center
Cleveland, Ohio 44135

E-1970

SUMMARY

The corrosion of nickel base superalloy, U-700, by molten Na_2MoO_4 has been studied in the temperature range 750° to 950° C. After an induction period, the rate of corrosion is linear and catastrophic corrosion is observed. The induction period is shown to be associated with the attainment of a minimum MoO_3 activity in the melt, which corresponds to the equilibrium MoO_3 activity for the reaction, $2MoO_3(\ell) + Mo = 3MoO_2(s)$. A mechanism is proposed to describe the catastrophic nature of corrosion, which involves transport of Ni^{++} through the melt resulting in formation of NiO at the melt-gas interface and basic fluxing of Cr_2O_3. The effect of the amount of Na_2MoO_4 on the corrosion kinetics has also been studied. Evaporation studies and the thermodynamic calculations for the Na_2MoO_4 - MoO_3 system have shown that the activity of MoO_3 is reduced considerably when dissolved in Na_2MoO_4, thus causing a sharp decrease in the rate of evaporation of MoO_3 from a Na_2MoO_4 - MoO_3 melt.

INTRODUCTION

Hot corrosion in aircraft combustion turbines is associated with the deposition of Na_2SO_4 on the blade and vane surfaces. The mechanism of hot corrosion of superalloys and coating systems have been studied by several investigators in the recent past (refs. 1 to 4). In general, the superalloys,

*NRC-NASA Resident Research Associate.

depending on the chemical composition, exhibit two different forms of corrosion; (1) accelerated corrosion, (2) catastrophic corrosion (ref. 1). The accelerated corrosion is associated with the formation of sulfides in the alloy, which increases the Na_2O activity of the Na_2SO_4 melt. The basic melt dissolves the protective oxides, thus causing accelerated corrosion. This form of corrosion has been observed for alloy systems containing no refractory elements, e.g., W, Mo, V.

Catastrophic corrosion has been observed in laboratory tests for alloy systems containing the refractory elements, i.e., W, Mo, and V. Goebel, Pettit and Goward (ref. 1) have postulated the acidic fluxing mechanism, in which the refractory metal oxides (MoO_3, WO_3, V_2O_5) dissolve in the Na_2SO_4 melt and thus increase the acidity of the salt melt. The acidified Na_2SO_4 melt then dissolves the other oxides like NiO, Al_2O_3, CoO, etc., thus resulting in catastrophic corrosion. Goebel and Pettit (ref. 6) have also shown that the presence of Na_2SO_4 is not essential in inducing catstrophic corrosion in the alloys containing refractory elements. In their studies, catastrophic corrosion could also be induced by Na_2WO_4. Catastrophic corrosion can also be induced by passing MoO_3 vapor over the Na_2SO_4 coated sample, as has been observed by Peters, et al. (ref. 5), and Goebel and Pettit (ref. 6). Bourhis and St. John (ref. 7) have shown that the catastrophic corrosion of superalloys containing Mo is due to fluxing by MoO_3, which is formed at the scale-metal interface. Studies in this laboratory (refs. 3 and 8) have shown that all the Na_2SO_4 was converted to Na_2CrO_4 much before the onset of catastrophic corrosion for superalloys containing Mo. The onset of catastrophic corrosion was marked by the conversion of Na_2CrO_4 to Na_2MoO_4, and frequently the scale-metal interface showed a Mo rich layer. The catastrophic corrosion was associated with the fluxing by a Na_2MoO_4 - MoO_3 mixture. Although it is well established that the catastrophic corrosion of superalloys containing Mo is due to the formation of Na_2MoO_4 and a Na_2MoO_4 - MoO_3 mixture, the mechanisms of the catastrophic corrosion are not clear. The present study is, therefore, aimed at understanding the mechanism of corrosion by Na_2MoO_4 at elevated temperatures.

EXPERIMENTAL

The alloy studied was cast U-700 (composition in weight percent = Cr 14.3, Co 15.0, Mo 4.1, Ti 3.56, Al 4.28, Ni balance). The test samples were coupons, approximately of size 23.5 by 10.8 by 2.3 mm with a hangdown hole in one end. All surfaces were glass bead blasted to give a uniform surface finish. The coupons were cleaned ultrasonically in trichloroethylene, detergent, distilled water, acetone and alcohol and then dried in an oven at 120° C. The samples were coated with Na_2MoO_4 by air brushing a saturated solution of the salt onto the coupons which were heated on a hot plate to 200° C. A few experiments were also conducted with a coating of either MoO_3 or a Na_2MoO_4 - MoO_3 mixture. The compound MoO_3 is not highly soluble in water. Therefore, for experiments in which a coating MoO_3 was desired, a slurry of MoO_3 in water was made and the slurry was air brushed onto the coupons. For a coating of the Na_2MoO_4 + MoO_3 mixture, the slurry of MoO_3 was first air brushed onto the coupons, and then Na_2MoO_4 was sprayed onto the MoO_3 coated sample. The corrosion experiments were performed in a vertical tube furnace. The flow of oxygen was downward at 100 cm min^{-1}. Continuous gravimetric measurements were made with a microbalance. The temperature range of interest in the present studies is 750° to 950° C. The test samples, corroded for different lengths of time, were washed in hot distilled water and the solution was analyzed for various water soluble elements. The corroded samples were examined by metallography, SEM and electron probe micro analysis.

RESULTS

Kinetics. - Corrosion tests were carried out for Na_2MoO_4 coated U-700 samples under various conditions, the principal variables being the amount of Na_2MoO_4 and temperature. Figure 1 shows the schematic of the corrosion kinetics, which is valid for all the temperatures studied. The weight gain versus time curve can be characterized by four distinct stages; (1) induction period, (2) period of catastrophic corrosion, during which the weight gain versus time curve is linear, (3) period of decelerating corrosion, (4) period of parabolic oxidation, during which the rate of corrosion is nearly the same as that of oxidation in O_2 only. In subsequent figures, while presenting

aspects of the corrosion kinetics, all four stages will not be shown. The last two stages, e.g., the period of decelerating corrosion and the period of parabolic oxidation will be frequently omitted. This is done primarily to maintain clarity in presenting the graphs.

The length of the induction period is dependent on both temperature and amount of Na_2MoO_4 on the sample. At a given temperature, the length of the induction period increases with an increase in the amount of Na_2MoO_4. This is shown in figure 2. From figure 2, it is also seen that the slope of the curve during the linear period of catastrophic corrosion is almost the same for all the doses of Na_2MoO_4. This is true for all the temperatures studied. Figure 2 also shows that at the same temperature the total weight gain or the extent of corrosion at the end of the period of decelerating corrosion increases with an increase in the amount of Na_2MoO_4.

The rate of corrosion during the linear period of catastrophic corrosion (as obtained from the slope of the straight line) decreases with a decrease in temperature. This is shown in figure 3, which shows the corrosion kinetics at different temperature for a fixed amount of Na_2MoO_4. As mentioned earlier, the rate of corrosion during the linear period of catastrophic corrosion is the same irrespecive of the amount of Na_2MoO_4. The temperature dependence of the length of the induction period is a strong function of the amount of Na_2MoO_4. Table I shows the length of the induction period at different temperatures as a function of the amount of Na_2MoO_4. For low doses (~1 mg/cm^2), the length of the induction period decreases with a decrease in temperature. At 750° C, virtually no induction period was observed for this dose of Na_2MoO_4. For intermediate doses (~2.5 mg/cm^2), the length of the induction period decreases with a decrease in temperature, attains a minimum at 850° C, and increases again with a decrease in temperature. For heavy doses (~4.5 mg/cm^2), the length of the induction period increases with decrease in temperature.

For the same amount of Na_2MoO_4, the weight gain or the extent of corrosion at the end of the period of decelerating corrosion increases with a decrease in temperature. This is shown in figure 4, which gives the corrosion kinetics at 950° and 850° C for a dose of 0.49 mg/cm^2 Na_2MoO_4.

Chemical analysis. - The U-700 coupons, corroded for different lengths or time at 950° C, were washed with hot distilled water and chemically analyzed for various elements. The solubility of various compounds of NiO, Cr_2O_3 and Al_2O_3 with MoO_3 (e.g., NiO • MoO_3, Cr_2O_3 • MoO_3, Al_2O_3 • MoO_3) in water is presumed to be low. Thus no appreciable amounts of Ni, Co, Cr, or Al were detected in the water washed solution. However, Na_2MoO_4 is soluble in water and the compound MoO_3 is fairly soluble in water. Therefore the chemical analysis showed the presence of appreciable amounts of Na and Mo in the solution. The results of the chemical analysis are shown in figure 5 for two different amounts of Na_2MoO_4. The corresponding weight gain curves are also superimposed on the plot of soluble species versus time. Figure 5(b) shows that the Mo concentration in the solution increases slowly during the induction period, and the end of the induction period is marked by a rapid increase in the Mo concentration in the solution. The concentration of Mo continues to increase during the period of catastrophic corrosion, reaches a peak, and then decreases until the end of corrosion. The time, at which the concentration of Mo starts to decrease, coincides with the beginning of the period decelerating corrosion. The Na concentration in the water washed solution decreases continuously with the progress of time.

Corrosion by Na_2MoO_4 - MoO_3 mixture. - The results of the chemical analysis clearly demonstrates that the end of the induction period is associated with the addition of a certain amount of MoO_3 to the Na_2MoO_4 melt. To further confirm the role of MoO_3 in inducing catastrophic corrosion, additional experiments were conducted in which a slurry of MoO_3 was airbrushed on to the sample and above this, a Na_2MoO_4 layer was applied by airbrushing. The mixture applied corresponds to Na_2MoO_4 - 23 mole percent MoO_3. For comparison, the weight gain data for Na_2MoO_4 only are also presented in figure 6. It can be seen from figure 6 that when MoO_3 is added to the Na_2MoO_4 melt, the induction period decreases considerably. These results further demonstrate that addition of MoO_3 to the Na_2MoO_4 melt is a prerequisite in inducing catastrophic corrosion in this alloy.

Scale morphology. - Figure 7 shows the top surface a sample coated with 1.5 mg/cm^2 of Na_2MoO_4 and corroded for 15 minutes at 950° C. This represents the initial period of corrosion. Figure 7 shows the top surface to

consist of the melt and a few NiO precipitates above the melt. Figure 8 shows a typical scale morphology, that is produced during the induction period. The outer oxide layer has spalled off at several places. The spalling tendency of the outermost scale decreases with a decrease in temperature. At 750° C, no spalling of the outmost oxide was observed during this period. Examination of outermost scale at higher magnification (fig. 8(b)) shows it to be NiO precipitates. It is believed that these NiO precipitates were formed during the initial period. The region where the outermost oxide layer had spalled from the surface consists of oxide grains and a melt in between the oxide grain (fig. 8(c)). This is indicative of melt penetration through the oxide. The cross section (fig. 8(d)) shows the scale to consist of two layers. The outermost layer is NiO, which is believed to be the precipitates formed during the initial period. The inner scale is porous and EDAX analysis shows the scale to consist of all the elements in the alloy, e.g., Ni, Co, Cr, Ti, Al. However, the scale appears to be rich in Cr and Ti. EDAX analysis also shows the presence of Na and Mo in the inner scale layer. The presence of Na and Mo in the inner scale layer further demonstrates that melt penetrates the oxide in this layer. It is presumed that melt penetration occurs along the pores in the oxide.

For samples corroded for a length of time corresponding to that of the period of catastrophic corrosion, thick porous oxide scale was produced. The thick external porous scale completely spalled of on cooling for corrosion experiments at high temperatures, e.g., 950° and 900° C. The spalling tendency decreases with a decrease in temperature, and at 750° C, the spalling was minimum. Therefore to obtain the details of the complete scale during the period of catastrophic corrosion, the cross section of the samples, corroded at 750° C, were examined. Figure 9 shows the scale morphology produced during the early stage of catastrophic corrosion. The top surface consists of NiO and shows a large number blisters (fig. 9(a)). The cross section through the blister (fig. 9(b)) shows the blisters to be formed by lifting of the scale by a melt at localized sites, thus resulting in pitting type of corrosion. The details of the cross section and the X-ray maps for various elements are shown in figure 10. The X-ray maps of the important elements, e.g., Ni, Cr and Mo are only shown. The other elements, Na, Ti, Al are present in small amounts, and X-ray maps for these elements are not shown in order to maintain simplic-

ity and emphasize the primary constituents. Co is usually observed to be present where Ni is, and therefore not shown in the X-ray maps. The X-ray maps in figure 10 show the outermost oxide layer to be primarily NiO. Beneath this NiO layer there is a layer consisting of Cr_2O_3 + NiO. This layer also contains Al, Ti and Co. These two layers, towards the scale-gas interface, were formed during the induction period (see fig. 8(d)). These oxide layers are lifted off the alloy surface by the formation of a thick Mo rich molten layer, which is seen as a solidified melt in the S • E • Image. EDAX analysis of this solidified melt layer shows the presence of Na, suggesting that this layer is a Na_2MoO_4 - MoO_3 mixture. As seen from the X-ray maps, the melt layer contains Ni, which is believed to be Ni dissolved in the melt. Just above the layer of solidified melt, there are precipitates consisting primarily of NiO and small amount of Cr_2O_3. Beneath the melt, there is a layer of oxide (main constituents Cr_2O_3 + NiO) on the alloy surface. A thin Mo rich layer is seen at the top of this oxide which is believed to be MoO_2(s). X-ray diffraction showed the presence of MoO_2(s) in the corroded sample.

The scale morphology during the period of catastrophic corrosion and after a time period longer than that in figure 10 is shown in figure 11. A pitting type of corrosion morphology is evident from figure 11, and the pit is seen to consist of a Na_2MoO_4 - MoO_3 melt (Na not shown). Ni and Cr are also observed to be there inside the pit. A thick porous oxide layer can be seen above the pit. The porous oxide layer consists of primarily NiO, and a small amount of Cr_2O_3. The outermost part of the scale, e.g., the NiO and Cr_2O_3 layer at the scale-gas interface in figure 10, have spalled off from the surface and cannot be seen in figure 11. Examination of the scale-metal interface (fig. 11(b)) shows a thin layer of oxide (~2 μm) to be present just beneath the pit. The detailed examination of the pit (fig. 12(a)) shows it to be Na_2MoO_4 - MoO_3 melt (Na not shown in the X-ray maps) containing dissolved Ni. Cr inside the pit is present as discrete Cr_2O_3 precipitates dispersed through the melt (fig. 12(b)).

The pitting type of corrosion morphology is observed at all temperatures during the period of catastrophic corrosion. Figure 13 shows the typical scale morphology at 950° C during the period of catastrophic corrosion. The

features are the same as that of 750° C, e.g., a pit consisting of Na_2MoO_4-MoO_3 melt with dissolved Ni and discrete Cr_2O_3 precipitates and a thin oxide layer at the pit-alloy interface. However, the external porous oxide layer had spalled off while cooling.

From the thermogravimetric results it is known that at lower temperatures, 750° and 850° C, a very long time is required for the corrosion to come to an end. Therefore the cross section of a sample, corroded at 950° C, for a time period corresponding to the end of the period of deccelerating corrosion will be examined. Figure 14 shows such a cross section and the X-ray maps for various elements. The pitting type of corrosion morphology is still observed. However, the pit no longer consists of a thick Na_2MoO_4 - MoO_3 liquid with dissolved Ni and discrete Cr_2O_3 precipitates. Now, the pit consists of only discrete NiO and Cr_2O_3 precipitates. All the MoO_3 or compounds of Mo appear to have disappeared from the pit. A layer of NiO + Cr_2O_3 is observed beneath the pit. The examination of the scale-metal interface at a higher magnification shows internal Al_2O_3 stringers, which were not observed in the cross section during the induction period and the period of catastrophic corrosion. These internal Al_2O_3 stringers are typical of the scale morphology for the alloy U-700, oxidized in air or O_2 without any salt being present.

DISCUSSION

The thermogravimetric results have shown that corrosion of U-700 beneath a Na_2MoO_4 melt involves a period of catastrophic corrosion, during which the rate of corrosion is linear and significantly higher than the rate of oxidation in O_2 alone. A linear rate of corrosion or accelerated corrosion is due to the development of a non-protective corrosion product layer. One of the ways by which a protective corrosion product layer cannot be developed beneath a layer of molten salt is the dissolution of the oxides in the melt. This is the conventional fluxing process, originally proposed by Bornstein and Decrescente (ref. 2) and later modified by Goebel, Pettit and Goward (ref. 1), to describe the hot corrosion of nickel base superalloys. In the fluxing process, the oxides are dissolved at the salt-oxide interface and again reprecip-

itated at the salt-gas interface. The dissolution is either basic or acid depending on the Na_2O activity in the melt. Rapp and Goto (ref. 9) have proposed a model in which the fluxing process requires a negative solubility gradient at the salt-oxide interface for the oxide in question.

Thermodynamic consideration. - In order to determine the corrosion mechanism, it is instructive to examine the fluxing process beneath the Na_2MoO_4 melt. For clarity the calculations will be presented only at 1200 K and for oxides of Ni and Cr. Similar to that for Na_2SO_4, the dissolution of the oxides in the Na_2MoO_4 melt is dependent on the Na_2O activity in the melt. The Na_2O activity in the Na_2MoO_4 melt is governed by the equilibrium conditions for the reaction:

$$Na_2MoO_4(\ell) = Na_2O(\ell) + MoO_3(\ell) \tag{1}$$

$$K_{(1)\ 1200\ K} = 3.17\times10^{-15} = \frac{{}^{a}Na_2O \cdot {}^{a}MoO_3}{{}^{a}Na_2MoO_4} \tag{2}$$

Where $K_{(1)}$ is the equilibrium constant for reaction (1), ${}^{a}Na_2O$, ${}^{a}MoO_3$ and ${}^{a}Na_2MoO_4$ are the activity of Na_2O, MoO_3 and Na_2MoO_4 in the melt, respectively. Rapp and his coworkers (refs. 10 and 11) have determined the solubility of various oxides as a function of ${}^{a}Na_2O$ in the Na_2SO_4 melt, and this is shown schematically in figure 15. Figure 15 exhibits a solubility minima at a certain Na_2O activity in the melt. For salts other than Na_2SO_4 the slopes of the acid and basic dissolution lines are expected to remain the same, although the curves might sift upward or downward depending on the thermodynamic stability of the products of dissolution of the oxides in the salt. However, the Na_2O activity, at which the solubility minima is obtained is expected to be the same for different salts.

From Gupta and Rapp's (ref. 11) measurement of the solubility of NiO in molten Na_2SO_4 as a function of ${}^{a}Na_2O$ at 1200 K, the solubility minima lies at ${}^{a}Na_2O$ equal to 10^{-10}. Assuming also for the Na_2MoO_4 melt that the solubility minima lies at the same Na_2O activity, according to equation (2) this would correspond to ${}^{a}MoO_3$ in the melt equal to 3.17×10^{-5}. From Stroud and Rapp's (ref. 10) measurement of the solubility of Cr_2O_3 in

molten Na_2SO_4, the solubility minima, for oxygen pressure of 1 atm, lies somewhere around Na_2O activity equal to 10^{-14}. From equation (2) this would correspond to ${}^{a}MoO_3$ in the melt equal to 0.25. The activity of MoO_3 in the melt is determined by the thermodynamic properties, e.g., partial molar properties of MoO_3 in the Na_2MoO_4 - MoO_3. Appendix B gives the details of the estimation of the thermodynamic properties of the Na_2MoO_4 - MoO_3 system from a study of the Na_2MoO_4 - MoO_3 phase diagram and rate of evaporation of the Na_2MoO_4 - MoO_3 mixture. The acidic fluxing mechanism requires that the MoO_3 activity in the melt must be greater than that corresponding to the solubility minima in the solubility versus - log ${}^{a}Na_2O$ plot. Thus for the acidic dissolution of NiO, the ${}^{a}MoO_3$ in the melt must be greater than 3.17×10^{-5} at 1200 K, and from the MoO_3 activity data in appendix B, this would correspond to approximately 10 mole percent MoO_3 in the melt. Similarly, for the acidic dissolution of Cr_2O_3, the ${}^{a}MoO_3$ in the melt must be greater than 0.25 and this would correspond to approximately 80 mole percent MoO_3 in the melt. Thus acidic dissolution of NiO is possible with addition of small amounts of MoO_3 to the melt, whereas dissolution of Cr_2O_3 requires addition of large amounts of MoO_3 to the melt.

Fluxing mechanism based on O_2 transport through melt. - According to the acidic fluxing mechanism, as has been proposed by Goebel and Pettit (ref. 1), and by Fryburg, et al. (ref. 3), to explain the role of molybdenum in the hot corrosion process, the oxides (NiO, Cr_2O_3, Al_2O_3) dissolve at the melt-oxide interface. It has been assumed that the oxides are formed at the melt-oxide interface. The driving force for the dissolution and reprecipitation process is the concentration gradient of MoO_3, $({}^{dC}MoO_3/dX)$, at the melt-oxide interface. The evaporation studies and the thermodynamic calculations for the Na_2MoO_4 - MoO_3 melt (appendixes A and B) show that the rate of evaporation of MoO_3 is considerably reduced when dissolved in Na_2MoO_4. The vaporization of MoO_3 would only be important at high concentration of MoO_3. Thus the concentration of MoO_3 in the melt would continue to rise with the progress of time, thereby reducing the magnitude of the driving force $({}^{dC}MoO_3/dX)$, at the melt-oxide interface. The magnitude of the driving force is continuously reduced with the progress of time until the rate of formation of MoO_3 at the melt-oxide interface becomes equal to the rate of evaporation of MoO_3 at the melt-gas interface. After this time period, the

concentration gradient of MoO_3 across the melt remains constant and therefore, the rate of dissolution-precipitation reaction would remain constant. In terms of weight gain, this would mean an initial high rate of weight gain, the rate decreasing with time until a steady state is reached during which the rate of weight gain remains constant. The rate of weight gain during the steady state would be less than the initial rate. The experimentally observed thermogravimetric curves show just the opposite of this e.g., the rate of weight gain during the linear period of catastrophic corrosion is higher than the initial rate. In the above analysis it has been assumed that the oxides formed at the melt-alloy interface are non-protective because of the dissolution of oxides in the melt.

In the mechanism, in which acidic dissolution of oxides takes place at the melt-oxide interface with subsequent reprecipitation at a distance away from this interface, the oxides are formed at the melt-oxide interface. This requires the transport of O_2 through the melt to the salt-oxide interface, where oxidation of Mo, Ni, Cr, Al takes place. The maximum flux of O_2 through the melt is given by the expression,

$$J = D \frac{C_o}{\delta} \tag{3}$$

where

J flux, moles/cm^2-sec
D diffusion of coefficient of O_2 in the Na_2MoO_4 melt, cm^2/sec
C_o solubility of O_2 in the melt, moles/cm^3
δ thickness of the melt, cm

The measurement of weight gain gives the flux of O_2 and thus, the maximum weight gain for different melt thicknesses can be calculated from equation (3). Anderson (ref. 12) has measured the solubility of O_2 in the molten Na_2SO_4, which is about 2×10^{-7} moles/cm^3 at 900° C. The solubility of O_2 in molten salts is governed by the equilibrium criteria for the reactions (ref. 12):

$$Na_2O + \frac{1}{2} O_2 = Na_2O_2 \tag{4}$$

$$Na_2O + O_2 = 2NaO_2 \quad (5)$$

In the present studies, the chemical analysis of the corroded samples shows that MoO_3 is being continuously added to the melt, thereby decreasing the Na_2O activity in the melt. Therefore the solubility of molecular O_2 in a Na_2MoO_4 - MoO_3 melt is expected to be lower than the measured value for the solubility in molten Na_2SO_4. However, for a conservative estimate of the maximum flux of O_2 through the melt, it can be assumed that the solubility of molecular O_2 in Na_2MoO_4 is the same as that in Na_2SO_4. Using the value of $2x10^{-7}$ mole/cm^3 for the solubility of O_2 in molten Na_2MoO_4, and $5x10^{-5}$ cm^2/sec (ref. 9) for the diffusivity of O_2 in molten Na_2MoO_4, the maximum weight gain for melt thicknesses of 10, 50 and 100 μm are calculated to be 1.15, 0.23 and 0.115 mg/cm^2/hr, respectively at 900° C. From thermogravimetric measurements, the weight gain during the linear period of catastrophic corrosion is of the order of 1.261 mg/cm^2/hr. The cross section of the corroded sample during the period of linear corrosion at 900° C shows the depth of the pit to be about 80 to 100 μm. Thus weight gain calculated on the basis of maximum flux of O_2 through the melt is much less than the observed weight gain. Clearly, then, the acidic fluxing mechanism based on the transport of O_2 through the melt cannot account for the rapid weight gain observed during the linear period of catastrophic corrosion. However, this mechanism may be important during the initial period of corrosion.

Fluxing mechanism based on Mo^{+4}/Mo^{+6} Exchange reaction. - In oxides, Mo is known to exist in two different oxidation states, e.g., Mo^{+4} and Mo^{+6}. In the oxidation of Mo, a thin layer of MoO_2 is usually observed in between the Mo and the external MoO_3 layer. In a Na_2MoO_4 - MoO_3 melt, two different oxidation states of Mo are also possible, i.e., dissolved MoO_2 and MoO_3. Indeed, recent electrochemical studies by Hellstorm (ref. 13) have shown that in a Na_2SO_4 - Na_2MoO_4 melt, Mo can exist in oxidation states other than Mo^{+6}. Rapp and Goto (ref. 9) have proposed a hot corrosion mechanism, in which the melt can be an electronic conductor, if an ion exists in two different oxidation states. The electron conduction arises due to the valence change electron transfer mechanism. A similar mechanism has also been proposed by Luthra (ref. 14) for the transport of Co through the

Na_2SO_4 - $CoSO_4$ melt in low temperature hot corrosion process. Assuming that Mo exists in the Na_2MoO_4 - MoO_3 melt as Mo^{+6} and Mo^{+4}, (dissolved MoO_3 and MoO_2), the exchange reaction in the melt can be described by the reaction:

$$\underline{MoO_2} + \frac{1}{2} O_2 = \underline{MoO_3} \tag{6}$$

$$K_6 = \frac{{}^{a}MoO_3}{{}^{a}MoO_2 \cdot (P_{O_2})^{1/2}} \tag{7}$$

where ${}^{a}MoO_3$ and ${}^{a}MoO_2$ are the activity of MoO_3 and MoO_2 in the melt, respectively. Since the oxygen pressure at the melt-gas interface is higher than the melt-oxide interface, the concentration of Mo^{+6} species will be greater at the melt/gas interface, and the concentration of Mo^{+4} species will be greater at the melt-oxide interface. This would result in migration of Mo^{+6} inward from the melt-gas to the melt-oxide interface, and migration of Mo^{+4} outward from the melt-oxide interface. At the melt-oxide interface, the Mo^{+6} ions are reduced to Mo^{+4} by reaction with Mo, and at the melt-gas interface, Mo^{+4} ions are oxidized to Mo^{+6}. In a manner similar to that oxidation of Mo in O_2 alone (ref. 15), a thin layer of MoO_2(s) is assumed to be present at the alloy-melt interface. The oxidation of Mo beneath at Na_2MoO_4 - MoO_3 melt is schematically shown in figure 16. As shown in figure 16, MoO_3 is formed at the melt-gas interface. The reaction mechanism shown in figure 16 is equivalent to the following reactions:

At the melt-oxide interface: $\underline{2MoO_3}$ + Mo (diffusing through the oxide) = $\underline{3MoO_2}$ (8)

At the melt-gas interface: $\underline{3MoO_2} + 3/2\ O_2 = \underline{3MoO_3}$ (9)

At the salt-oxide interface, the melt is in equilibrium with solid MoO_2. Therefore, the minimum ${}^{a}MoO_3$ necessary for reaction (8) to proceed in the forward direction is governed by the equilibrium conditions for the reaction:

$$\underline{2MoO_3} + Mo = 3MoO_2(s) \tag{10}$$

$$K_{10} = \frac{\left(a_{MoO_{2(s)}}\right)^3}{\left(a_{MoO_{3(\ell)}}\right)^2 \cdot a_{Mo}} \qquad (11)$$

The activity of $MoO_2(s)$ is unity and assuming a_{Mo} to be unity, the equilibrium a_{MoO_3} for reaction (11) at 1200 K is calculated to be 1.695×10^{-5}. From the thermodynamics of the Na_2MoO_4 - MoO_3 melt (appendix B), the activity value of 1.695×10^{-5} corresponds to 10 mole percent MoO_3 in the melt. Thus reaction (8) will proceed in the forward direction after the MoO_3 concentration in the melt becomes equal to about 10 mole percent. As will be seen in a later section, the minimum a_{MoO_3} in the melt necessary for reaction (10) to go in the forward reaction is the basis for the existence of the induction period.

When the activity of MoO_3 in the melt becomes equal to the equilibrium MoO_3 activity for reaction (10), the MoO_3 concentration in the melt rises rapidly because of formation of MoO_3 by Mo^{+4}/Mo^{+6} exchange reaction (shown in fig. 16). Now MoO_3 component of the melt becomes the principal oxidizing species. The oxidation of Ni and Cr beneath the Na_2MoO_4 - MoO_3 melt is described by the following reaction:

$$MoO_3\ (\ell) + Ni = MoO_2\ (s) + NiO \qquad (12)$$

$$3MoO_3\ (\ell) + 2Cr = Cr_2O_3 + 3MoO_2\ (s) \qquad (13)$$

At 1200 K, the equilibrium MoO_3 activity in the melt for reaction (12) is calculated to be 3.99×10^{-3}. From the thermodynamics of the Na_2MoO_4 - MoO_3 melt (appendix B), this would correspond to approximately 50 mole percent MoO_3 in the melt. At 1200 K, the equilibrium MoO_3 activity in the melt for reaction (13) is calculated to be 3.89×10^{-9}. Thus formation of Cr_2O_3 requires a low MoO_3 concentration in the melt, whereas for oxidation of Ni, a considerable amount of MoO_3 must be added to the melt for reaction (12) to go in the forward reaction. At the melt-oxide interface, $MoO_2(s)$ is in equilibrium with $MoO_2(\ell)$, and the dissolved MoO_2 diffuses to the melt-gas interface where it is oxidized to MoO_3. Thus reactions (12) and (13) are self-sustaining.

At the melt-oxide interface, the acidic dissolution of oxides can take place by reactions:

$$NiO = Ni^{++} + O^{=} \tag{14}$$

$$Cr_2O_3 = 2Cr^{+++} + 3\ O^{=} \tag{15}$$

As mentioned earlier, the criteria for acidic dissolution is that the $^{a}MoO_3$ at the melt-oxide interface must be greater than that corresponding to the solubility minima in the solubility versus - $\log {}^{a}Na_2O$ curve. It has been shown earlier that for the acidic dissolution of Cr_2O_3 to occur, the MoO_3 activity at the melt-oxide interface must be greater than 0.25. From the thermodynamics of the Na_2MoO_4 - MoO_3 melt (appendix B), this corresponds to about 75 mole percent MoO_3. The MoO_3 concentration in the melt is governed by two competing factors, the rate of formation of MoO_3 and rate of evaporation of MoO_3. The concentration of MoO_3 in the melt would remain constant when the rate of formation of MoO_3 became equal to the rate of evaporation. For a melt consisting of 75 mole percent MoO_3, the rate of evaporation of MoO_3 could be high, and it is doubtful whether the melt can attain such a high concentration of MoO_3.

The chemical analysis of the corroded samples at 950° C showed the maximum MoO_3 concentration to be approximately 40 mole percent. Therefore the acidic dissolution of Cr_2O_3 would not be expected at the melt-oxide interface. Instead, at the melt-oxide interface basic dissolution of Cr_2O_3 would take place by the reaction:

$$Cr_2O_3 + \frac{3}{2}\ O_2 + 2O^{=} = 2CrO_4^{=} \tag{16}$$

Because of the positive gradient of MoO_3 at the melt-oxide interface, the gradient of oxide ion activity is negative at the melt-oxide interface. Therefore the oxide solubility gradient is negative at the melt-oxide interface and the Rapp-Goto criterion for fluxing is satisfied, thus leading to the reprecipitation of Cr_2O_3 at some distance away from the melt-oxide interface. The scale morphology in figures 11 and 12 shows Cr_2O_3 precipitates inside the melt and in the outer precipitate layer. This is believed to be due to the basic fluxing of Cr_2O_3.

At 1200 K, the activity of MoO_3 in the melt must be greater than 3.12×10^{-5} for acidic dissolution of NiO to take place. This value of $^{a}MoO_3$ in the melt corresponds to approximately 10 mole percent MoO_3 in the melt. The $^{a}MoO_3$ in the melt necessary for the acidic dissolution (3.17×10^{-5}) is of the same order of magnitude as the minimum $^{a}MoO_3$ necessary at the melt-oxide interface for reaction (10) to proceed in the forward direction (1.695×10^{-5}). Therefore, the acidic dissolution of NiO can take place at the melt-oxide interface as described by reaction (14). However, the activity gradient for MoO_3 is positive at the melt-oxide interface because of formation of MoO_3 at the melt-gas interface. Therefore the reprecipitation of the dissolved oxides would not take place. Instead the melt will be gradually saturated with Ni^{++}. The overall MoO_3 concentration of the melt increases with time, thus the concentration of dissolved Ni^{++} would increase with time. The scale morphologies and the X-ray maps of the corroded samples (figs. 11 and 12) show dissolved Ni in the melt, suggesting the acidic dissolution of NiO. However, the scale morphology in figures 11 and 12 also show a porous NiO layer above the melt at the melt-gas interface, which cannot be explained based on acidic fluxing of NiO at the melt-oxide interface.

In order to explain the formation of porous NiO at the salt-gas interface, the following mechanism is proposed. The mechanism is again based on Mo^{+6}/Mo^{+4} exchange reaction and is schematically shown in figure 17. At the melt-oxide interface, Ni reacts with Mo^{+6}, which is migrating from the melt-gas interface, to form Mo^{+4} and Ni^{++} by the following reactions:

$$Ni = Ni^{++} + 2e \tag{17}$$

$$Mo^{+6} + 2e = Mo^{+4} \tag{18}$$

At the melt-gas interface, the Ni^{++} ions are oxidized to NiO, and Mo^{+4} ions are oxidized to Mo^{+6} by the reactions:

$$Mo^{+4} = Mo^{+6} + 2e \tag{19}$$

$$Ni^{++} + 2e + 1/2O_2 = NiO \tag{20}$$

At the melt-oxide interface, the reduction of Mo^{+6} to Mo^{+4} generates the $O^{=}$ ions, which are consumed by the reaction:

$$Cr_2O_3 + \frac{3}{2} O_2 + O^{=} = 2CrO_4^{=} \qquad (21)$$

The $CrO_4^{=}$ ions are reprecipitated to Cr_2O_3 by reverse of reaction (21) at some distance away from the melt-oxide interface inside the melt and at the melt-gas interface. The reverse of reaction (21) generates $O^{=}$ which combines with Mo^{+6} to form MoO_3. Thus reactions (17) to (21) are self-sustaining. A steady state condition is attained when the melt is saturated with Ni^{++}, after which the concentration gradient of Ni^{++} acorss the melt remains constant. Under steady state conditions a linear rate of weight gain is observed. The melt is saturated with Ni^{++}; presumably when the $NiMoO_4$ concentration of the melt corresponds to the liquidus in the $NiMoO_4$ rich portion of the hypothetical Na_2MoO_4 - $NiMoO_4$ phase diagram, which is the maximum amount of $NiMoO_4$ that a fixed quantity of Na_2MoO_4 can dissolve. At the melt-gas interface NiO can also react with MoO_3 to form solid $NiMoO_4$.

Thermodynamic calculations for the oxidation of Ni beneath a Na_2MoO_4 - MoO_3 melt showed that the concentration of MoO_3 at the melt-oxide interface must be greater than approximately 50 mole percent for the oxidation of Ni to take place according to reaction (12). It is unlikely that such a high concentration of MoO_3 would be attained at the melt-oxide interface. However, according to the mechanism proposed in figure 17, NiO need not be formed at the melt-oxide interface. Instead, NiO is formed at the melt-gas interface by formation of Ni^{++} at the melt-alloy/oxide interface and subsequent transport to the melt-gas interface. Because of the higher diffusivity of Ni^{++} in the melt, the rate of oxidation can be substantially increased. The mechanisms proposed in figure 17 is consistent with the generalized criteria for fluxing that has been proposed by Luthra (ref. 15).

The mechanism, proposed in figure 17 also applies to corrosion beneath a melt consisting of MoO_3 only. This was confirmed by examining the cross section of samples coated with MoO_3 and oxidized at elevated temperatures. Figure 18 shows that scale morphology and the features are observed to be sim-

ilar to those observed for corrosion beneath a Na_2MoO_4 melt. The scale morphology in figure 18 also suggests that even for the melt consisting of MoO_3 only, acidic dissolution of Cr_2O_3 can not take place at the melt-oxide interface. (The MoO_3 activity gradient is positive at the melt-oxide interface and acidic dissolution of Cr_2O_3 would not have produced the Cr_2O_3 precipitates inside the melt.)

In order for the mechanism proposed in figure 17 to be operative, the alloy must contain Cr because the $O^{=}$ ions (generated at the melt-oxide interface due to reduction of Mo^{+6} to Mo^{+4}) react with Cr_2O_3 to form $CrO_4^{=}$. The precipitation of $CrO_4^{=}$ to Cr_2O_3 and $O^{=}$ takes place at the melt-gas interface. If oxidation of Mo^{+4} to Mo^{+6} at melt-gas interface by reaction (19) is to occur, $O^{=}$ needs to be supplied to maintain electrical neutrality. To confirm this, a coupon of nickel was coated with 2.62 mg/cm^2 of Na_2MoO_4 + 0.5 mg/cm^2 MoO_3 and oxidized at 950° C. The weight gain was only 4.08 mg/cm^2 at the end of 18 hr. For U-700, the weight gain for the same time period was of the order of 36 mg/cm^2. Brenner (ref. 16) has studied the oxidation of Fe-Mo alloys and Fe-Mo alloys containing Cr and has shown that Fe-Mo alloys containing up to 20 percent Mo were not oxidized very rapidly in air at 1000° C. However, addition of Cr to the alloy caused catastrophic oxidation. This is consistent with our mechanism and clearly shows that the alloy must contain Cr for the accelerated corrosion to occur.

Sequence of corrosion reactions. - When the alloy is oxidized beneath the Na_2MoO_4 melt, during the transient stage of oxidation, oxides of all the elements in the alloy are formed beneath the melt, the oxidants being supplied by the transport of O_2 through the melt. MoO_3 is also formed on the alloy surface, which dissolves in the Na_2MoO_4 melt at the melt-oxide interface. The activity of MoO_3 at the melt-oxide interface is high and therefore acidic fluxing of oxides takes place. Because of the negative gradient in the MoO_3 activity at the melt-oxide interface, the dissolved oxide is reprecipitated at the salt-gas interface. Discussion of fluxing process beneath the Na_2MoO_4 melt showed that this mechanism can not account for the experimentally observed weight gain and the nature of the thermogravimetric curve. Therefore this process of dissolution-reprecipitation is only of importance during the initial period of corrosion.

The results of the chemcial analysis (fig. 5) show that the MoO_3 content of the melt increases slowly during the induction period and the end of induction period is marked by a rapid increase in the MoO_3 content of the melt. Consideration of the oxidation and fluxing mechanism beneath the Na_2MoO_4 melt showed that rapid oxidation of Mo takes place when Mo oxidizes according to the Mo^{+4}/Mo^{+6} exchange reaction as shown in figure 16. For the oxidation of Mo to occur by this scheme it was also shown that the MoO_3 activity in the melt must attain a minimum value. The minimum $^{a}MoO_3$ in the melt was calculated to be 1.695×10^{-5} (10 mole percent MoO_3) at 1200 K. However, the mechanism by which MoO_3 is being added to the melt during the induction period is not clear. Shores (ref. 17), based on transport calculations through the melt, has concluded that for IN738 the oxide which developed beneath a Na_2SO_4 melt was porous and the melt could fill these pores. A similar situation is likely to exist for the oxides beneath a Na_2MoO_4 melt. This is evidenced in figure 8(c), which shows the melt penetration through the oxide. Also the EDAX analysis of the inner scale in figure 8(d) shows the presence of Na and Mo in the scale. Thus, during the induction period, it is believed that a porous nonprotective scale is formed and the melt is dispersed in the pores through out the oxide. The melt is also in contact with the alloy at the oxide-alloy interface, where oxidation of Ni and other alloying elements takes place. The oxidant is supplied by the transport of O_2 through the melt and therefore the rate of MoO_3 formation is expected to be slow because of slow transport of O_2 through a tortuous path of pores filled with the melt. The oxidation process continues by the transport of O_2 through the melt until the MoO_3 activity in the melt becomes equal to the equilibrium $^{a}MoO_3$ for reaction (10). The amount of dissolved MoO_3 required to attain a given MoO_3 activity in the Na_2MoO_4 - MoO_3 melt increases with an increase in the amount of Na_2MoO_4. This leads to an increase in the length of the induction period with an increase in the amount of Na_2MoO_4.

At the end of the induction period, the MoO_3 concentration of the melt rises rapidly, and the formation of MoO_3 takes place according to the mechanism shown in figure 16, i.e., by Mo^{+4}/Mo^{+6} exchange reaction. Cr_2O_3 and Al_2O_3 are formed beneath the melt by reaction with the MoO_3 component of the melt. The acidic dissolution of Ni and basic fluxing of Cr_2O_3 take

place as shown in figure 17. The formation of NiO takes place at the melt-gas interface. The O_2 required for basic dissolution of Cr_2O_3 by reaction (21) can also be supplied by the MoO_3 component of the melt. The exact mode of dissolution of Al_2O_3 is not clear. The concentration of Al in the alloy is so small that it is assumed to have no major effect on the fluxing process. The dissolution of Co is expected to take place in a manner similar to that of Ni. The thermogravimetric curves in figures 2 and 3 show a gradual transition from the end of the induction period to the beginning of the linear period of catastrophic corrosion. During this transition period, the Ni^{++} (also Co^{++}) concentration in the melt increases with time until the melt is saturated with Ni^{++}. The flux of Ni^{++} through the melt is a product of the diffusivity of Ni^{++} in the melt and the concentration of Ni^{++} in the melt. Therefore, the rate of oxidation (also the rate of weight gain) increases with time because of the increase in Ni^{++} concentration with time during the transition period. When the melt is saturated with Ni^{++}, a steady state condition is achieved and the concentration gradient of Ni^{++} across the melt remains constant. This results in a linear relationship between the weight gain and time.

It must be noted that the dissolution and reprecipitation reactions shown in figure 17 are self-sustaining because oxidation of Mo^{+4} at the melt-gas interface regenerates the MoO_3. However, the oxidation of the Mo component of the alloy, by the mechanism shown in figure 16, generates MoO_3 at the melt-gas interface thus increasing the MoO_3 concentration in the melt. On the other hand, MoO_3 is lost to the atmosphere by evaporation at the salt-gas interface. Evaporation studies for Na_2MoO_4 (appendix A) have shown that Na_2MoO_4 is volatile, the rate of vaporization being 0.03 and 0.035 $mg/cm^2/hr$ at 900° and 950° C, respectively. In a Na_2MoO_4 - MoO_3 melt, the evaporation of Na_2MoO_4 increases the activity of MoO_3 in the melt, thus resulting in an increase in the rate of evaporation of MoO_3. Thus there are two competing factors, rate of evaporation of MoO_3 and rate of generation of MoO_3 (due to the oxidation of Mo) which determine the MoO_3 concentration in the melt at a given time. Thermodynamic calculations and evaporation studies (appendixes A and B) have shown that the rate of evaporation of MoO_3 is considerably reduced when dissolved in Na_2MoO_4 melt, and the evaporation of MoO_3 becomes significant only at high MoO_3 concentra-

tions in the melt. Therefore, MoO_3 is continuously added to the melt, as seen in figure 5, until the concentration of MoO_3 becomes such that the rate of generation of MoO_3 by oxidation of Mo in the alloy becomes equal to the rate of evaporation of MoO_3. For convenience let us designate this time period as t_1. At this time, a steady state can be attained and the MoO_3 concentration of the melt would remain constant. However, Na_2MoO_4 is continuously evaporated from the melt, which effectively increases the activity of MoO_3 in the melt, thereby increasing the rate of evaporation of MoO_3. Therefore after time t_1, the MoO_3 concentration in the melt decreases with time. With a decrease in MoO_3 activity in the melt, the solubility of Ni^{++} in the melt decreases, thus decreasing the concentration of Ni^{++} in the melt. Some dissolved Ni^{++} is precipitated as oxides because of the decrease in solubility. Also the reduction in Ni^{++} concentration in the melt reduces the rate of transport of Ni^{++} through the melt, thereby reducing the rate of oxidation. This is the period of decelerating corrosion, which starts at time t_1.

When all the Na_2MoO_4 is vaporized, the accelerated corrosion comes to a halt because a molten layer is no longer present. (Any MoO_3 left will evaporate quickly because of the unit activity of MoO_3.) The rate of evaporation of Na_2MoO_4 at 950° C was measured to be 0.035 $mg/cm^2/hr$ (appendix A). For a dose of 0.73 mg/cm^2 Na_2MoO_4, assuming unit activity, it would take 20.8 hr for all the Na_2MoO_4 to vaporize and the corrosion to stop. From the thermogravimetric data in figure 2, for a dose of 0.73 mg/cm^2, it takes 25 hr for the corrosion to stop at 950° C, which is longer than the time period calculated based on the evaporation of Na_2MoO_4 (20.8 hr). This discrepancy is due to the dissolution of MoO_3 in the melt, which also reduces the activity of Na_2MoO_4. Because the catastrophic corrosion stops when all the Na_2MoO_4 has evaporated, the length of the period of catastrophic corrosion is a function of the amount of Na_2MoO_4. The larger the amount of Na_2MoO_4, the longer is the length of the time period during which the material corrodes. Therefore the total weight gain at the end of the period of decelerating corrosion increases with an increase in the amount of Na_2MoO_4.

Effect of temperature. - It is seen from table I that temperature has a major effect on the length of the induction period. As mentioned earlier, the end of the induction period corresponds to the time at which the MoO_3 activity in the melt becomes equal to the equilibrium $^{a}MoO_3$ for reaction (10). The equilibrium MoO_3 activity for reaction (10) decreases with decreasing temperature. For example, the equilibrium MoO_3 activity for reaction (10) was calculated to be 1.695×10^{-5}, 4.72×10^{-6}, 8.61×10^{-7} at 1200, 1123, and 1023 K, respectively. The rate of oxidation of alloying elements and the rate of transport of O_2 through the melt decrease with decreasing temperature. Thus, there are two competing factors, thermodynamic and kinetic, which determine the length of the induction period. For low doses, and at lower temperatures (750° and 850° C), the MoO_3 formed during the first few minutes may increase the MoO_3 activity of the melt to that required for reaction (10) to proceed. Thus at 850° and 750° C, for low doses practically no induction period was observed. For high doses, more MoO_3 has to be added to the melt to increase the MoO_3 activity to that of equilibrium. The MoO_3 added to the melt during the initial period thus may not increase the activity to a sufficiently high value to allow reaction 10 to proceed. Thus the transport of O_2 through tortuous melt filled paths in the oxide and the rate of oxidation at the alloy scale interface becomes rate determining. These rates decrease with a decrease in temperature, thereby increasing the length of the induction period with a decrease in temperature. At intermediate doses, because of thermodynamic and kinetic factors, the length of the induction period would be minimum at certain intermediate tem- perature, which was observed to be the case at 850° C.

As mentioned earlier, the corrosion comes to a halt when all the Na_2MoO_4 is vaporized. The rate evaporation of Na_2MoO_4 decreases with temperature. Thus for the same amount of Na_2MoO_4, the length of the time period, during which material undergoes accelerated corrosion, increases with decreasing temperature.

SUMMARY AND CONCLUSIONS

Catastrophic corrosion of nickel base superalloys containing Mo can be caused by formation of Na_2MoO_4. The period of catastrophic corrosion is

preceded by an induction period. It has been shown that the activity of MoO_3 in the melt must attain a certain mimimum value before the onset of catastrophic corrosion. This is related to the equilibrium MoO_3 activity in the melt for the reaction $2MoO_3(\ell) + Mo = 2MoO_2(s)$. The length of the induction period corresponds to the time required for the attainment of equilibrium MoO_3 activity in the melt for the above reaction. The length of the induction period is a strong function of temperature and the amount of Na_2MoO_4. At the end of the induction period, MoO_3 is formed by a Mo^{+6}/Mo^{+4} exchange reaction in the melt, in which Mo^{+6} is reduced to Mo^{+4} by reaction with Mo at the melt-oxide interface, and Mo^{+4} is oxidized to Mo^{+6} at the melt-gas interface.

During the period of catastrophic corrosion, Ni is dissolved as Ni^{++} at the melt-oxide/alloy interface by reaction with Mo^{+6} thus forming Mo^{+4}. Simulaneously basic dissolution of Cr_2O_3 also takes place at this interface. The Ni^{++} ions are oxidized to NiO at the melt-gas interface, and $CrO_4^{=}$ ions are converted to Cr_2O_3 and $O^{=}$ at a distance away from the melt-oxide interface. The dissolution-precipitation reaction is self-sustaining. The catastrophic corrosion stops when all the Na_2MoO_4 has vaporized.

The present study has shown that the rate of evaporation of MoO_3 is considerably reduced when dissolved in Na_2MoO_4. Thus evaporation of MoO_3 would not be significant in actual gas turbine situations, as has been proposed by several investigators (refs. 7 and 18). In the situation encountered in a burner rig, and probably in actual gas turbines under hot corrosion conditions, there is continuous deposition of the Na_2SO_4. The Na_2SO_4 reacts with MoO_3 at the melt-gas interface, and in effect acts as a sink for MoO_3. The mode of fluxing will then be a complex function of the rate of formation of MoO_3, rate of reaction between MoO_3 and Na_2SO_4, and the rate of deposition of Na_2SO_4. The details of the fluxing mechanism in which there is continuous deposition of Na_2SO_4 is the subject of further investigation at this laboratory.

APPENDIX A

EVAPORATION OF Na_2MoO_4, MoO_3 and Na_2MoO_4 - MoO_3 MIXTURE

To determine the rate of evaporation, the desired compound or mixture was placed in platinum crucible and the rate of evaporation was measured by measuring the weight loss in the microbalance. The flow rate of O_2 was maintained the same as that in the corrosion experiments, e.g., 100 cm min^{-1}.

The rate of evaporation of Na_2MoO_4, MoO_3 and Na_2MoO_4 - MoO_3 mixtures are shown in table II. It can be seen that MoO_3 is highly volatile, the rate of evaporation increasing with temperature. It is interesting to note that the rate of evaporation of MoO_3 is drastically reduced when dissolved in Na_2MoO_4. For example, for a Na_2MoO_4 - 13 mole percent MoO_3 mixture, assuming ideal solution, $^{a}Na_2MoO_4 = 0.87$ and $^{a}MoO_3 = 0.13$. Thus under ideal solution conditions, 22.04 mg of MoO_3 and 0.253 mg of Na_2MoO_4 would vaporize in 1 hr. However, the total amount evaporating is 0.25 mg in 1 hr, which is much less than that which would have evaporated under ideal solution conditions.

The disadvantage of measuring the rate of evaporation from a crucible containing the salt is that the surface area is unknown, therefore, the rates cannot be directly related to the corrosion measurements. No measurement of the rate of evaporation of MoO_3 could be carried out on a Pt coupon of known surface area because of the high volatility of MoO_3. For example at 900° C, all the MoO_3, that could be applied to a Pt coupon, evaporated within the first 2-3 minutes of the start of the experiment. The rate of evaporation of Na_2MoO_4 from a sample of known surface area could be carried out by air-brushing Na_2MoO_4 on to Pt coupons, and measuring the weight loss from the Na_2MoO_4 coated coupons. Such measurements gave vaporization rate of 0.035 $mg/cm^2/hr$ at 950° C and 0.03 $mg/cm^2/hr$ at 900° C.

APPENDIX B

THERMODYNAMICS OF THE Na_2MoO_4 - MoO_3 SYSTEM

There is no experimental data on the thermodynamic properties of Na_2MoO_4 - MoO_3 melts. However, the thermodynamic properties can be estimated from the relevant binary phase diagram. The estimation of thermodynamic properties from the phase diagram has been extensively used for molten salts and slag systems (ref. 19). The Na_2MoO_4 - MoO_3 phase diagram is taken from reference 20 and shown in figure 19. The phase diagram does not show the existence of any solid solution between Na_2MoO_4 - MoO_3. The solid-liquid equilibrium can be described by the reaction:

$$s \rightarrow \ell \tag{B-1}$$

$$\Delta G^{\circ}_{s \rightarrow \ell} = \frac{\Delta H^{\circ}_{fusion}(T_m - T)}{T_m} = -RT \ln a_{\ell} \tag{B-2}$$

where ΔG° = Gibbs free energy change for reaction (B-1), $\Delta H^{\circ}_{fusion}$ = heat of fusion of the solid at the melting point. T_m = melting point, T = temperature along the liquidus line and a_{ℓ} is the activity of the component in the liquid in reference to the pure liquid as the standard state. The data calculated along the liquidus can be extrapolated to other temperatures by assuming that at a fixed composition, the partial heat of solution is independent of temperature (ref. 21).

Then,

$$RT_{\ell} \ln \nu_{\ell} = RT \ln \nu_T \tag{B-3}$$

$$a_T = x_{\ell} \cdot \nu_T \tag{B-4}$$

Where T_{ℓ} and ν_{ℓ} are the liquidus temperatures and activity coefficient at the liquidus, respectively, T and ν_T are the temperatures and activity co-efficients at the chosen temperature T, a_T is the activity at a temperature T for a composition corresponding to the liquidus composition, X_{ℓ} is the liquidus composition at temperature T_{ℓ}.

From Barin and Knacke's (ref. 22) test, the melting point and heat of fusion for MoO_3 are 1068 K and 11.507 kcal/mole, respectively. Using these data, the activity of MoO_3 at the liquidus in the MoO_3 rich portion of the phase diagram can be calculated from equation (B-2). The calculated values of ${}^{a}MoO_3$ at the liquidus composition for different temperatures is shown in table III. The activity of MoO_3 at other temperatures for compositions corresponding to the liquidus can be calculated from equation (B-3). From the MoO_3 rich side of the binary Na_2MoO_4 - MoO_3 phase diagram, the activity of MoO_3 can be determined only in the composition range $0.77 < {}^{X}MoO_3 < 1$, where ${}^{X}MoO_3$ is the mole fraction of MoO_3 in the melt.

For composition ranges other than $0.77 < {}^{X}MoO_3 < 1$, the MoO_3 activity in the melt can be estimated from the vaporization rate of Na_2MoO_4 - MoO_3 mixture (given in appendix A) and a study of the Na_2MoO_4 rich portion of the binary Na_2MoO_4 - MoO_3 phase diagram, which is described as follows. Let ${}^{p}{}^{\circ}Na_2MoO_4$ and ${}^{p}{}^{\circ}MoO_3$ be the equilibrium vapor pressure of Na_2MoO_4 and MoO_3, respectively, at unit activity. The rate of evaporation of Na_2MoO_4 and MoO_3 at unit activity can be expressed as:

$$ {}^{K}{}^{\circ}Na_2MoO_4 = h\left[{}^{p}{}^{\circ}Na_2MoO_4 - {}^{p}Na_2MoO_4 \quad (\text{ambient}) \right] \tag{B-5} $$

$$ {}^{K}{}^{\circ}MoO_3 = h\left[{}^{p}{}^{\circ}MoO_3 - {}^{p}MoO_3 \quad (\text{ambient}) \right] \tag{B-6} $$

Where ${}^{K}{}^{\circ}Na_2MoO_4$ and ${}^{K}{}^{\circ}MoO_3$ are the rate of evaporation of Na_2MoO_4 and MoO_3, respectively, h is the mass transfer coefficient, ${}^{p}Na_2MoO_4$ (ambient) and ${}^{p}MoO_3$ (ambient) are the partial pressure of Na_2MoO_4 and MoO_3 in the ambient, respectively. For the flow conditions used in the present experiments, ${}^{p}Na_2MoO_4$ (ambient) and ${}^{p}MoO_3$ (ambient) are assumed to be zero. Because all the evaporation studies were conducted under the same experimental conditions, i.e., same flow rate and specimen geometry, the mass transfer coefficient is assumed to be constant for all the experiments. In a Na_2MoO_4 - MoO_3 mixture, the equilibrium vapor pressure of Na_2MoO_4 and MoO_3 can be expressed as:

$$ {}^{P}Na_2MoO_4 = {}^{a}Na_2MoO_4 \cdot {}^{P}{}^{\circ}Na_2MoO_4 \tag{B-7} $$

$$ {}^{P}MoO_3 = {}^{a}MoO_3 \cdot {}^{P}{}^{\circ}MoO_3 \tag{B-8} $$

Where $^{P}Na_2MoO_4$ and $^{P}MoO_3$ are the equilibrium vapor pressure of Na_2MoO_4 and MoO_3, respectively in the Na_2MoO_4 - MoO_3 mixture, $^{a}Na_2MoO_4$ and $^{a}MoO_3$ are the activity of Na_2MoO_4 and MoO_3 in the melt, respectively. The rate of evaporation of the Na_2MoO_4 - MoO_3 mixture can be expressed as:

$$K^{\circ}Na_2MoO_4 - MoO_3 = {}^{a}Na_2MoO_4 \cdot K^{\circ}Na_2MoO_4 + {}^{a}MoO_3 \cdot K^{\circ}MoO_3 \qquad (B-9)$$

Thus, if $K^{\circ}Na_2MoO_4 - MoO_3$, $^{a}Na_2MoO_4$, $K^{\circ}Na_2MoO_4$ and $K^{\circ}MoO_3$ are known, $^{a}MoO_3$ at a given composition can be calculated from equation (B-9).

From appendix A, at 900° C, $K^{\circ}Na_2MoO_4$, $K^{\circ}MoO_3$, $K^{\circ}Na_2MoO_4 - MoO_3$ ($^{X}MoO_3 = 0.13$) were measured to be 0.291 mg/hr, 169.56 mg/hr and 0.245 mg/hr, respectively. From the Na_2MoO_4 rich side of the phase diagram, $^{X}MoO_3 = 0.13$ corresponds to liquidus temperature of 610° C. From Barin and Knacke's (B-4) text, the melting point and heat of fusion for Na_2MoO_4 are 962 K and 5.12 kcal/mole, respectively. Using this data, the activity of Na_2MoO_4 in the melt at 610° C at the liquidus composition ($^{X}MoO_3 = 0.13$) was calculated to be 0.786. From the activity data at 610° C, the activity of Na_2MoO_4 at 900° C for a melt consisting of Na_2MoO_4 - MoO_3 ($^{X}MoO_3 = 0.13$) was calculated to be 0.806. Substitution of this value of $^{a}Na_2MoO_4$ and the vaporization data for Na_2MoO_4, MoO_3, Na_2MoO_4 - MoO_3 ($^{X}MoO_3 = 0.13$) in equation (B-9) gives the value of $^{a}MoO_3$ ($^{X}MoO_3 = 0.13$) at 900° C to be 6.16×10^{-5}.

From appendix A, the rate of evaporation of a Na_2MoO_4 - MoO_3 mixture ($^{X}MoO_3 = 0.54$) is 0.75 mg/hr at 900° C. A liquid of this composition is not in equilibrium with solid Na_2MoO_4. Thus the activity of Na_2MoO_4 at this composition can not be obtained from a study of the Na_2MoO_4 rich portion of the binary phase diagram. For this liquid mixture ($^{X}MoO_3 = 0.54$), assuming that the activity of Na_2MoO_4 is the same as the mole fraction ($^{a}Na_2MoO_4 = 0.46$), and using the vaporization data for Na_2MoO_4, MoO_3, and Na_2MoO_4 - MoO_3 ($^{X}MoO_3 = 0.56$), the $^{a}MoO_3$ was calculated to be 3.63×10^{-3}. On the other hand by assuming that all the vaporization was due to the evaporation of MoO_3 only, the $^{a}MoO_3$ was calculated to be 4.42×10^{-3}. The two calculated values have the same order of magnitude, which is due to the rate of evaporation of MoO_3 being

much greater than the rate of evaporation of Na_2MoO_4 at this composition. The actual value for $^aMoO_3$ will lie somehwere in between these two values, and a value of $^aMoO_3$ equal to approximately $4x10^{-3}$ will not be unreasonable.

Table IV shows the $^aMoO_3$ values at 900° C for a range of composition. In the composition range $0.77 < {}^xMoO_3 < 1$, the $^aMoO_3$ was obtained by extrapolating the data from table III to 900° C by using equations (B-3) and (B-4). For other compositions, the activity values were obtained from the evaporation studies for the Na_2MoO_4 - MoO_3 mixture. Table V shows the $^aMoO_3$ values at 1200 K, which were obtained from table IV. From tables IV and V, it can be seen that the activity of MoO_3 is considerably reduced for low concentrations of MoO_3 in the melt.

REFERENCES

1. Goebel, J. A.; Pettit, F. S.; and Goward, G. W.: Mechanisms for the Hot Corrosion of Nickel-Base Alloys. Metall. Trans., vol. 4, Jan 1973, pp. 261-278.

2. Bornstein N. S.; and DeCrescente, M. A.: The Role of Sodium in the Acclerated Oxidation Phenomenon Termed Sulfidation. Metall. Trans., vol. 2, Oct. 1971, pp. 2875-2883.

3. Fryburg, G. C.; Kohl, F. J.; Stearns, C. A.; and Fielder, W. L.: Chemical Reactions Involved in the Initiation of Hot Corrosion of B-1900 and NASA-TRW VIA. J. Electrochem. Soc., vol. 129, No. 3, Mar. 1982, pp. 571-585.

4. Stringer, J.; and Whittle, D. P.: Metal-Slag-Gas Reactions and Processes. Z. A. Foroulis and W. W. Smeltzer, eds., The Electrochemical Society, Pennington, New Jersey, 1975, p. 665.

5. Peters, K. R.; Whittle, D. P.; and Stringer, J.: Oxidation and Hot Corrosion of Nickel-Based Alloys Containing Molybdenum. Corros. Sci., vol. 16, No. 11, Nov. 1976, pp. 791-804.

6. Goebel, J. A.; and Pettit, F. S.: Metal-Slag-Gas Reactions and Processes. Z. A. Foroulis and W. W. Smeltzer, eds., The Electrochemical Society, Pennington, New Jersey, 1975, p. 693.

7. Bourhis, Y.; and Saint-John, C.: Properties of High Temperature Alloys. Z. A. Foroulis and W. W. Smeltzer, eds., The Electrochemical Society, Pennington, New Jersey, 1977, p. 626.

8. Misra, A. K.; and Kohl, F. J.: Effect of the Amount of Na_2SO_4 on the High Temperature Corrosion of Udimet-700. NASA-TM 83459, 1983.

9. Rapp, R. A.; and Goto, K.S.: Second International Symposium on Molten Salts, J. Braunstein and J. R. Selman, eds., The Electrochemical Society, Pennington, New Jersey, 1981, pp. 159-171.

10. Stroud, William P.; and Rapp, Robert A.: The Solubilities of Chromic Oxide and α-Aluminum Oxide in Fused Sodium Sulfate at 1200 K. High Temperature Metal Halide Chemistry, D. L. Hildenbrand and D. D. Cubicciotti, eds., The Electrochemical Society, Pennington, New Jersey, 1978, pp. 574-94.

11. Gupta, Dilip K.; and Rapp, Robert A.: The Solubilities of NiO, Co_3O_4, and Ternary Oxides in Fused Na_2SO_4 at 1200 K. J. Electrochem. Soc., vol. 127, No. 10, Oct. 1980, pp. 2194-2202.

12. Anderson, Rolf E.: Solubility of Oxygen and Sulfur Dioxide Molten Sodium Sulfate and Oxygen and Carbon Dioxide in Molten Sodium Carbonate. J. Electrochem. Soc., vol. 126, No. 2, Feb 1979, pp. 328-334.

13. Hellstorm, E. E.: A Preliminary Study of the Redox Behavior of Tungstate and Molybdate Ions in Na_2SO_4 at 1203 K. Corros. Sci., vol. 23, No. 7, 1983, pp. 709-715.

14. Luthra, K. L.: Low Temperature Hot Corrosion of Cobalt-Base Alloys - Part II. Reaction Mechanism. Metall. Trans., vol. 13A, No. 10, Oct. 1982, pp. 1853-1864.

15. Hauffe, K.: Oxidation of Metals. Plenum Press, New York, 1965.

16. Brenner, S. S.: Catastrophic Oxidation of Some Molybdenum-Containing Alloys. J. Electrochem. Soc., vol. 102, No. 1, Jan. 1955, pp. 16-21.

17. Shores, D. A.: High Temperature Corrosion. R. A. Rapp, ed., National Association of Corrosion Engineers, 1983, p. 493.

18. Santoro, Gilbert J.: Hot Corrosion of Four Superalloys: HA-188, S-57, IN-617, and TD-NiCrAl, Oxid. Metals, vol. 13, No. 5, 1979, pp. 405-435.

19. Lumsden, John: Thermodynamics of Molten Salt Mixtures. Academic Press, New York, 1966.

20. Phase Diagrams for Ceramists. 1975 Supplement, E. M. Levin and H. F. McMurdie, eds., Am. Ceramic Soc. 1975, p. 93.

21. Charles, R. J.: Activities in Li_2O-, Na_2O-, and K_2O-SiO_2 Solutions. J. Am. Ceramic Soc., vol 50, No. 12, Dec 21, 1967, pp. 631-641.

22. Barin, I.; Knacke, O.; and Kubaschewski, O.: Thermochemical Properties of Inorganic Substances. Springer-Verlag, Berlin, 1977.

TABLE I. - LENGTH OF INDUCTION PERIOD

AT DIFFERENT TEMPERATURES

Amount of Na_2MoO_4, mg/cm^2	Temperature, °C	Length of the induction period, hr
1	950	12
	900	5
	850	1
	750	No induction period
2.5	950	40
	900	29
	850	10
	750	27
4.5	900	90
	850	140
	750	160

TABLE II. - RATE OF EVAPORATION OF Na_2MoO_4, MoO_3 AND Na_2MoO_4 - MoO_3 MIXTURE

Compound or mixture	Temperature, °C	Weight loss in 1 hr, mg
MoO_3	950	584
	900	169.56
	850	77.5
	750	15
Na_2MoO_4	900	.291
Na_2MoO_4 - MoO_3 (X_{MoO_3} = 0.13)	900	.245
Na_2MoO_4 - MoO_3 (X_{MoO_3} = 0.54)	900	.75
Na_2MoO_4 - MoO_3 (X_{MoO_3} = 0.8)	900	15.32

TABLE III. - ACTIVITY OF MoO_3 AT THE LIQUIDUS COMPOSITION IN THE MoO_3 RICH SIDE OF THE BINARY Na_2MoO_4 - MoO_3 PHASE DIAGRAM

Temperature, °C	Mole fraction of MoO_3, X_{MoO_3}	Activity of MoO_3, a_{MoO_3}
700	0.9	0.587
600	.8	.295
537	.77	.176

TABLE IV. - ACTIVITY OF MoO_3 IN THE Na_2MoO_4 - MoO_3 MELT AT 900° C

Mole fraction of MoO_3, X_{MoO_3}	Activity of MoO_3, a_{MoO_3}
0.13	6.16×10^{-5}
.54	4×10^{-3}
.77	0.277
.8	.380
.9	.631

TABLE V. - ACTIVITY OF MoO_3 IN THE Na_2MoO_4 - MoO_3 MELT AT 1200 K

Mole fraction of MoO_3, X_{MoO_3}	Activity of MoO_3, a_{MoO_3}
0.13	7.3×10^{-5}
.54	4.46×10^{-3}
.77	0.283
.8	.386
.9	.636

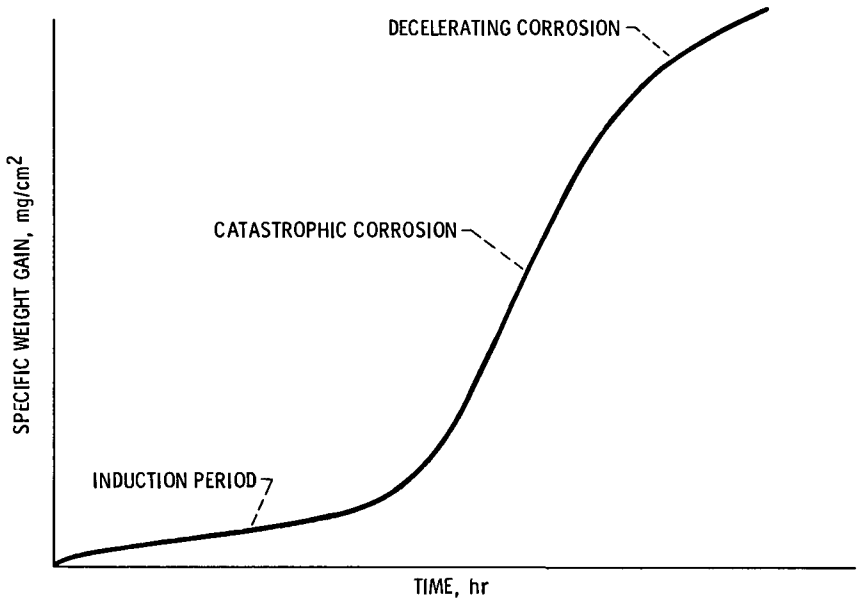

Figure 1. - Schematics of the corrosion kinetics.

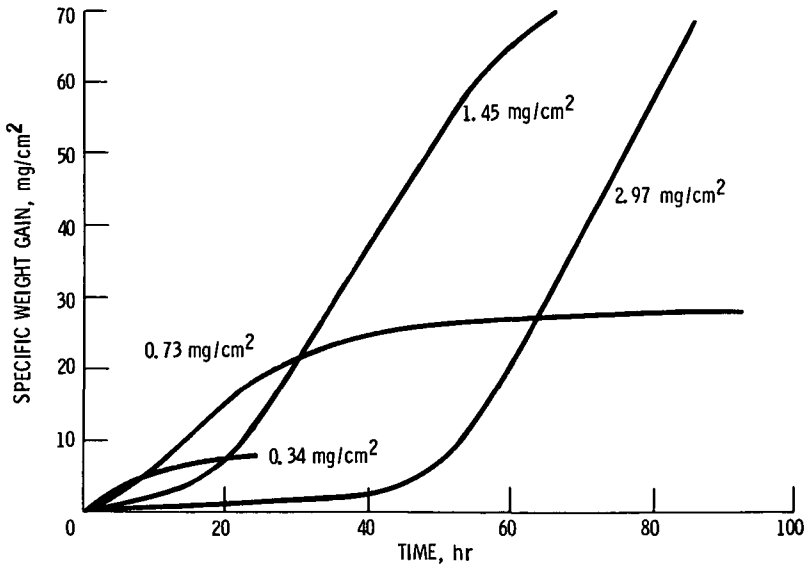

Figure 2. - Corrosion kinetics at 950° C as a function of the amount of Na_2MoO_4.

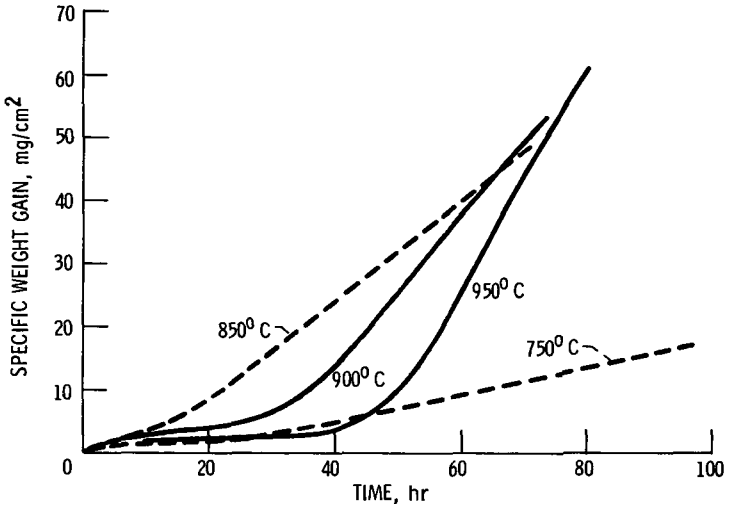

Figure 3. - Corrosion kinetics as a function of temperature for a dose of 2.5 mg/cm^2 Na_2MoO_4.

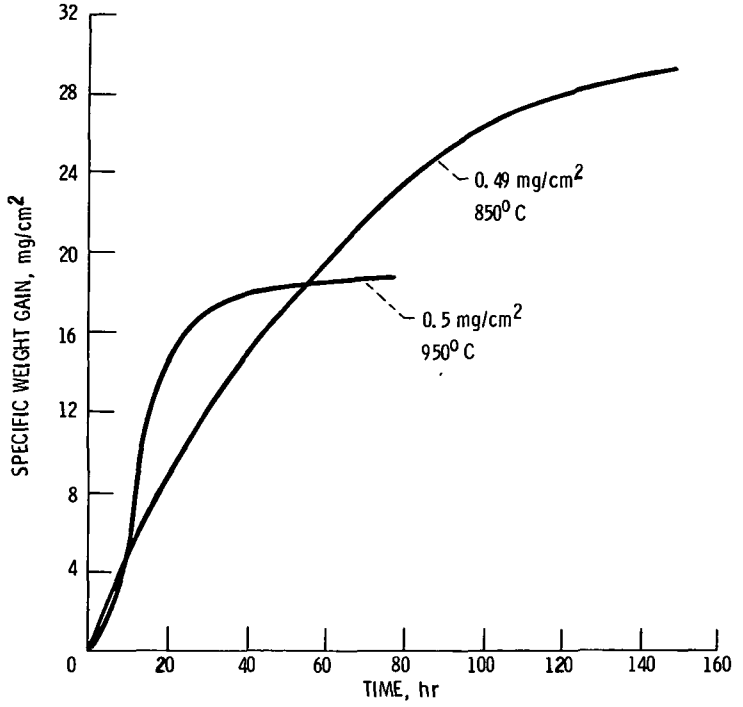

Figure 4. - Total weight gain as a function of temperature for a fixed amount of Na_2MoO_4.

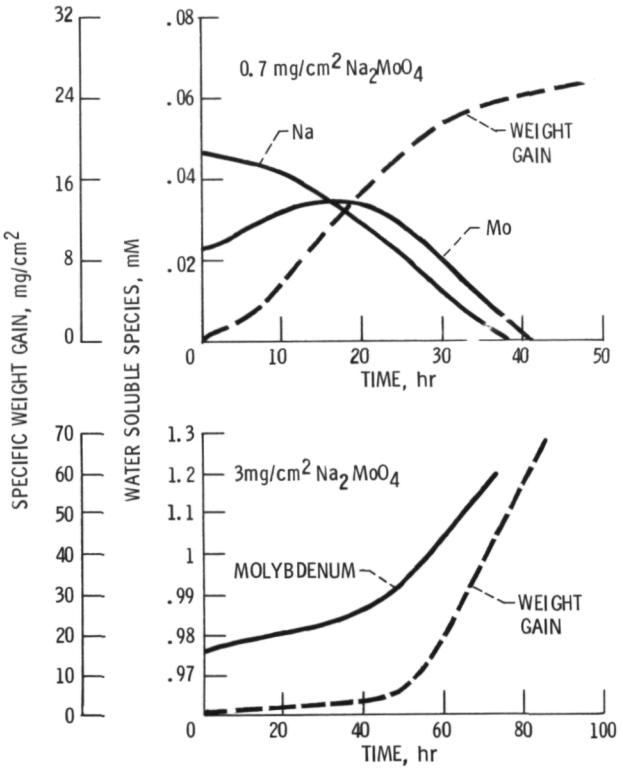

Figure 5. - Analysis of water soluble elements for the corroded sample at 950° C.

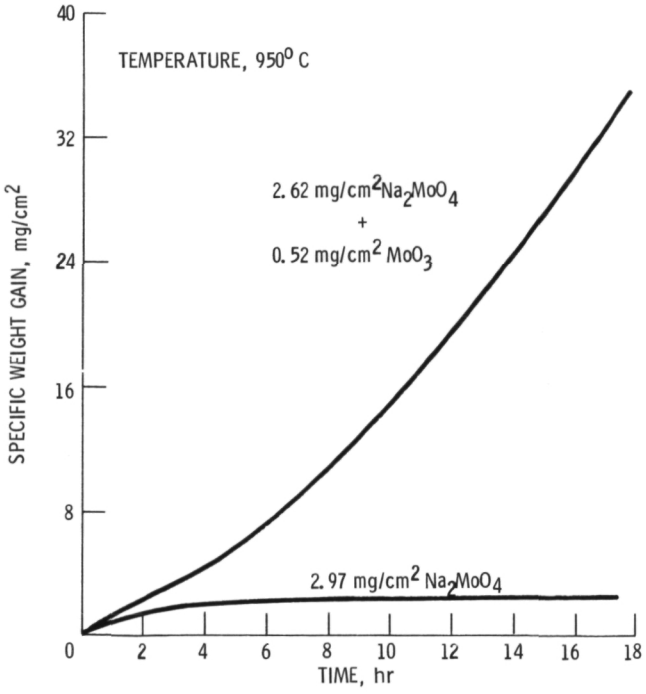

Figure 6. - Corrosion kinetics with a deposit of Na_2MoO_4 - MoO_3.

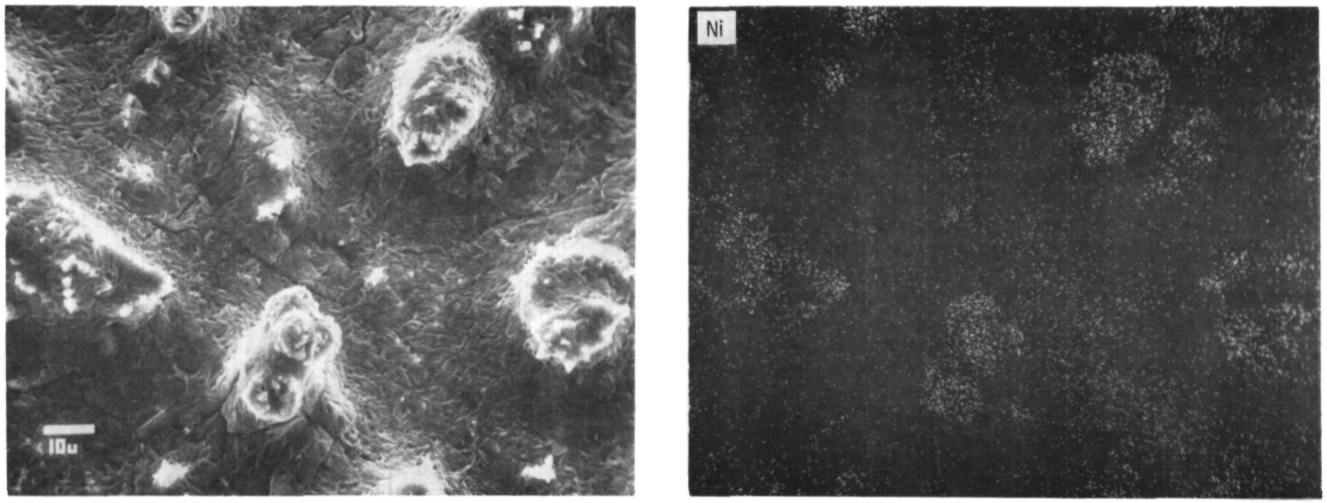

Figure 7. - Scale morphology during the initial period for U-700, coated with 1.5 mg/cm^2 Na_2MoO_4 and oxidized in 1 atm O_2 for 15 minutes at 950^0 C.

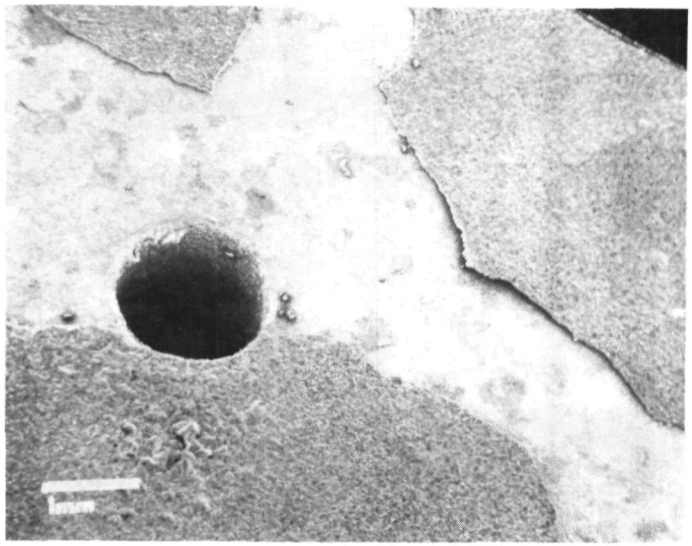

(a) Top surface.

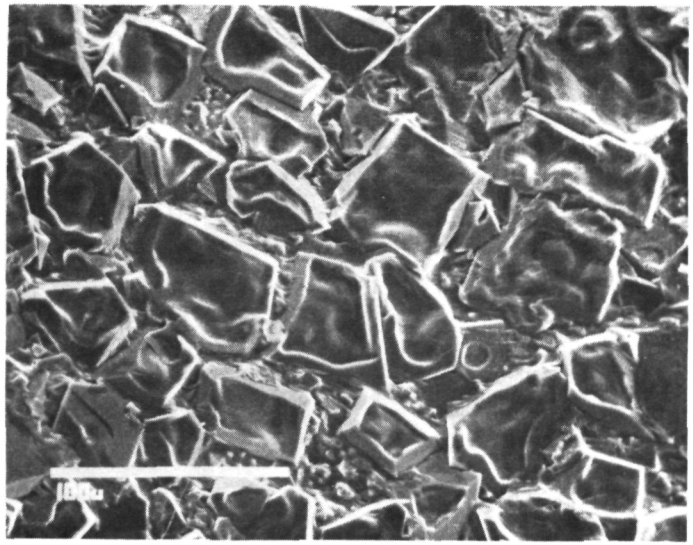

(b) Outermost oxide in (a), NiO.

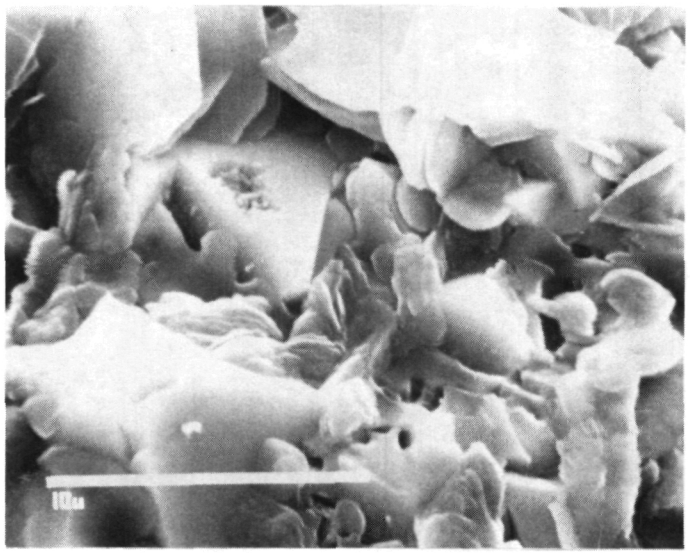

(c) Spalled region in (a), Oxide + Melt.

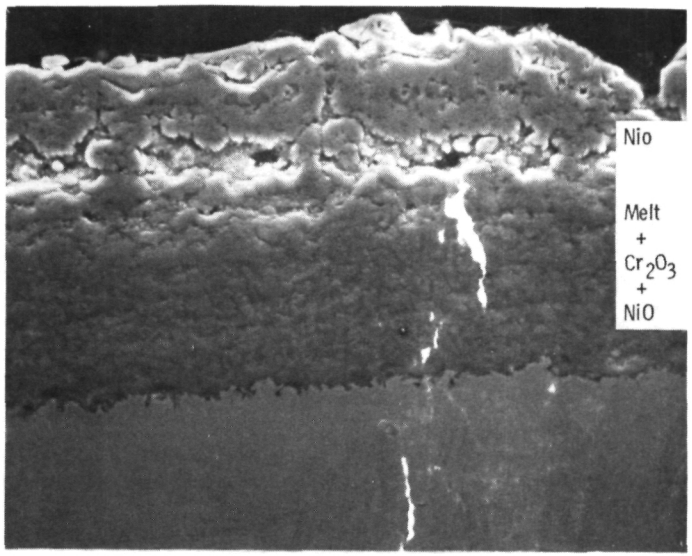

(d) Cross section.

Figure 8. - Scale morphology during the induction period, sample coated with 2.1 mg/cm^2 Na_2MoO_4 and oxidized for 20 hrs at 950^0 C.

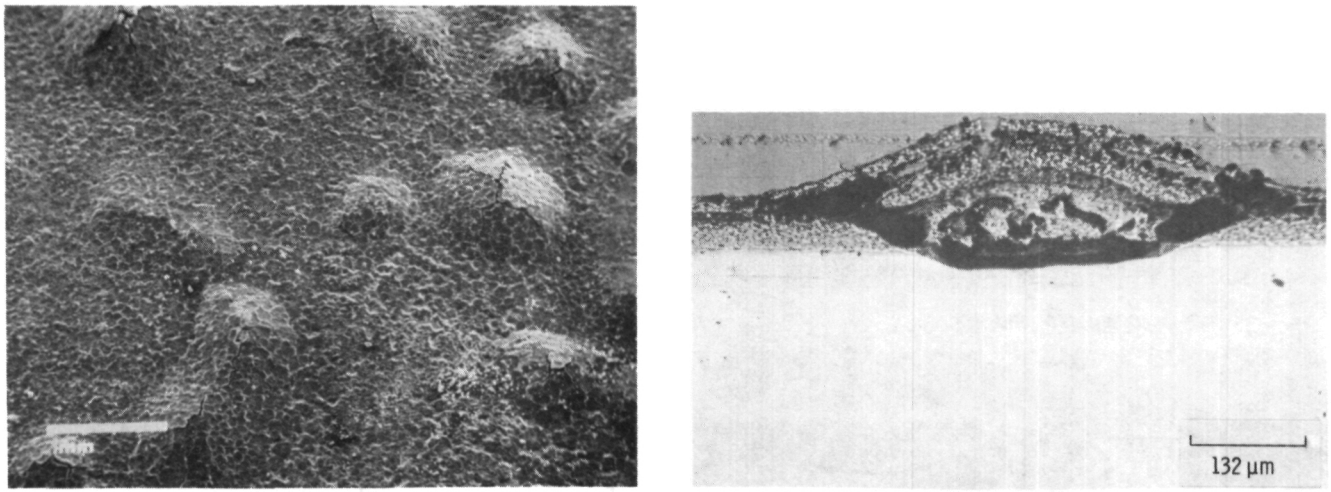

(a) Top surface.

(b) Cross section.

Figure 9. - Scale morphology during early stages of catastrophic corrosion: sample coated with 2.4 mg/cm^2 Na_2MoO_4 and oxidized in 1 atm O_2 for 60 hrs at 750^0 C.

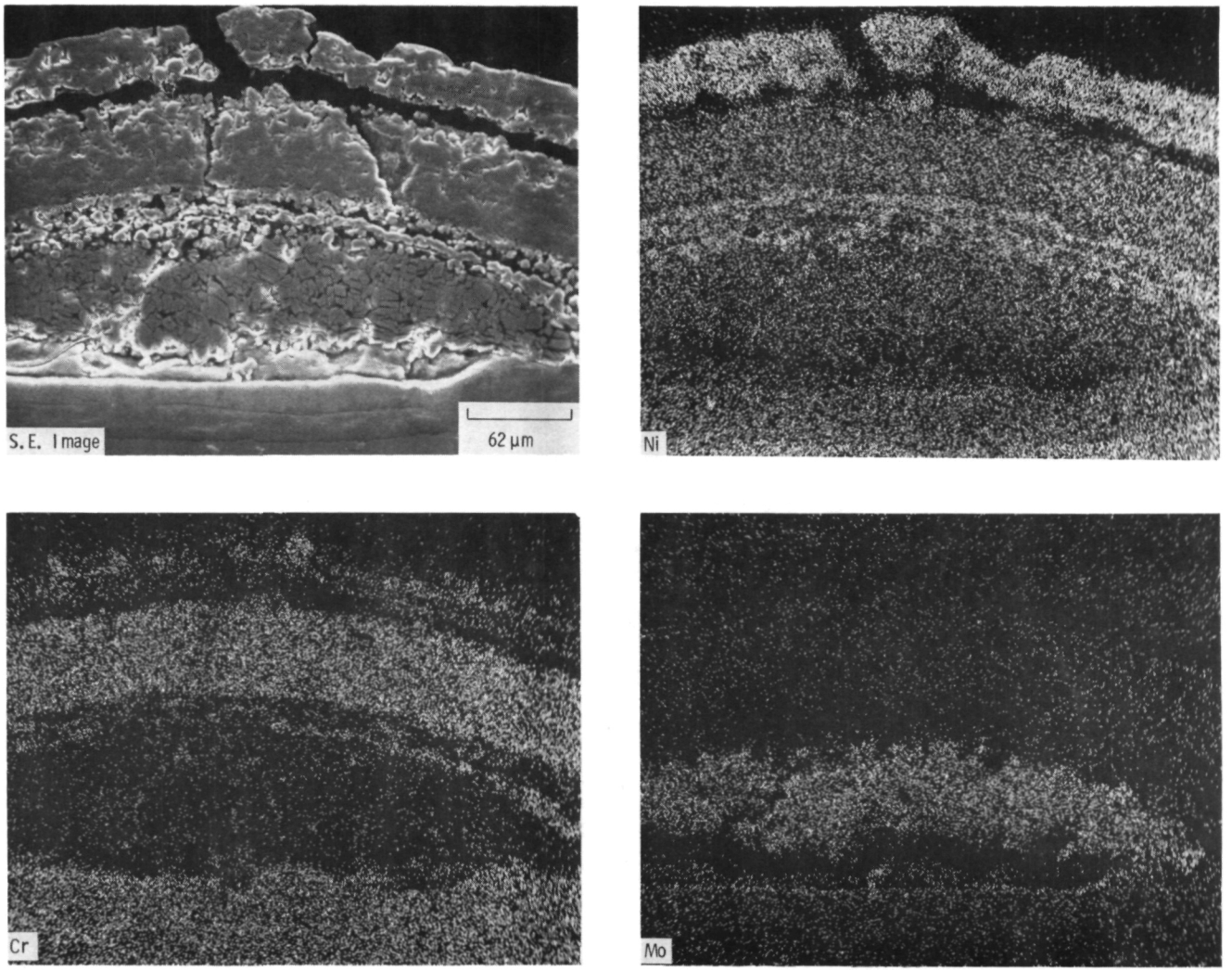

Figure 10. - S. E. image and X-ray maps for the cross-section shown in figure 9.

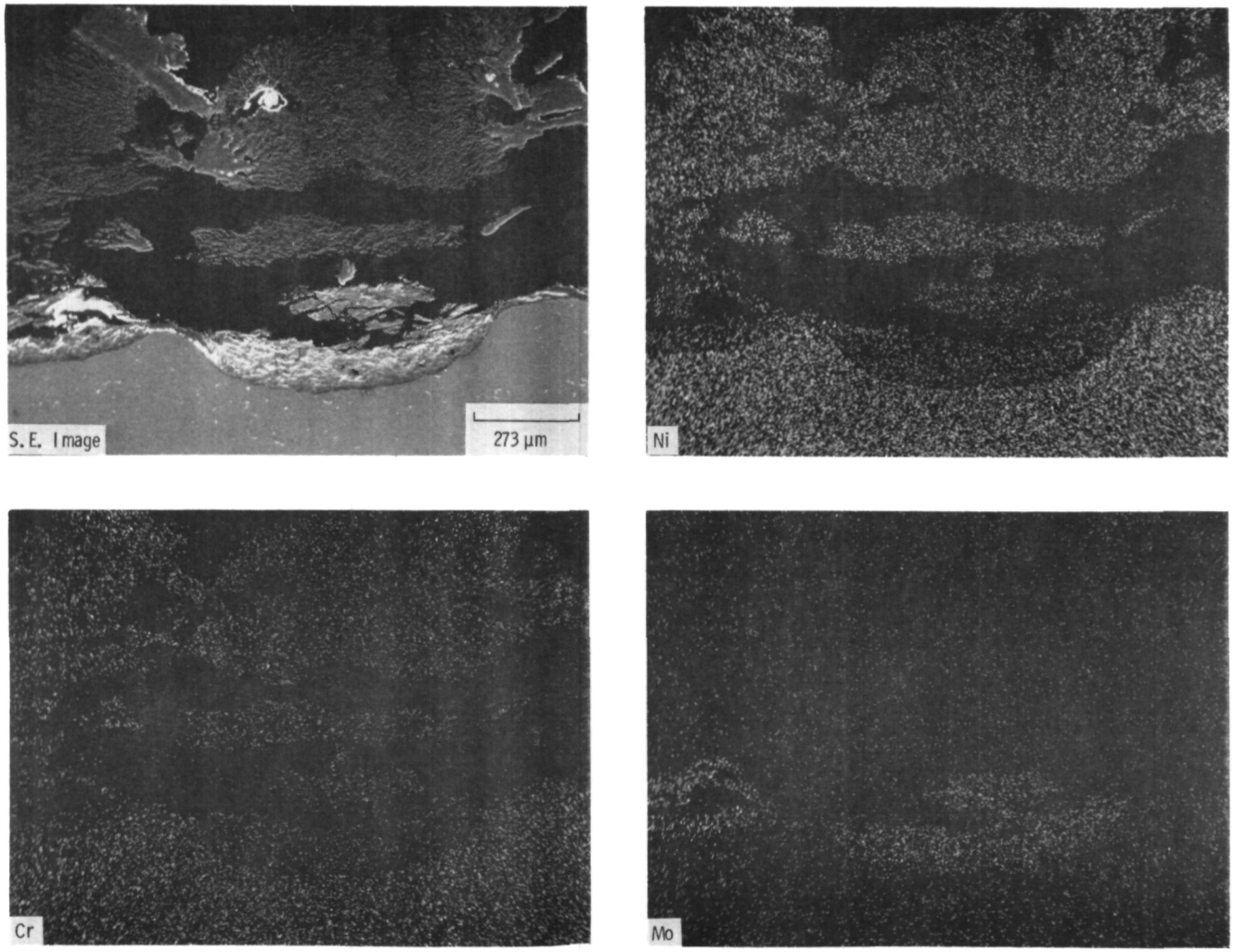

(a) S. E. image and X-ray maps for the pit.

Figure 11. - Scale morphology during advanced stage of catastrophic corrosion, sample coated with 0.985 mg/cm^2 Na_2MoO_4 and oxidized in 1 atm O_2 for 173 hrs at 750^0 C.

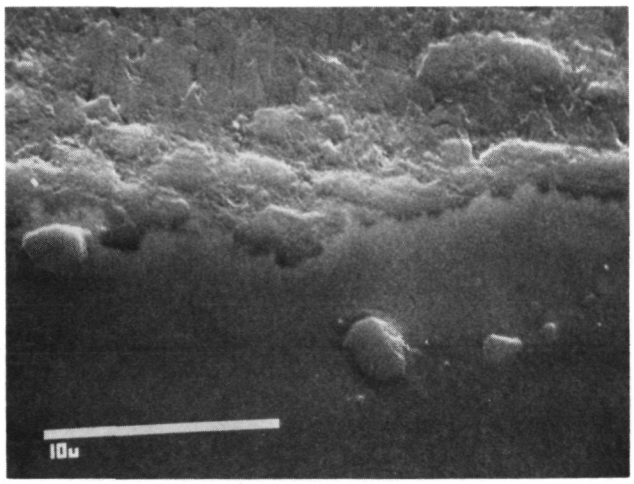

(b) Details of the scale-metal interface.
Figure 11. - Concluded.

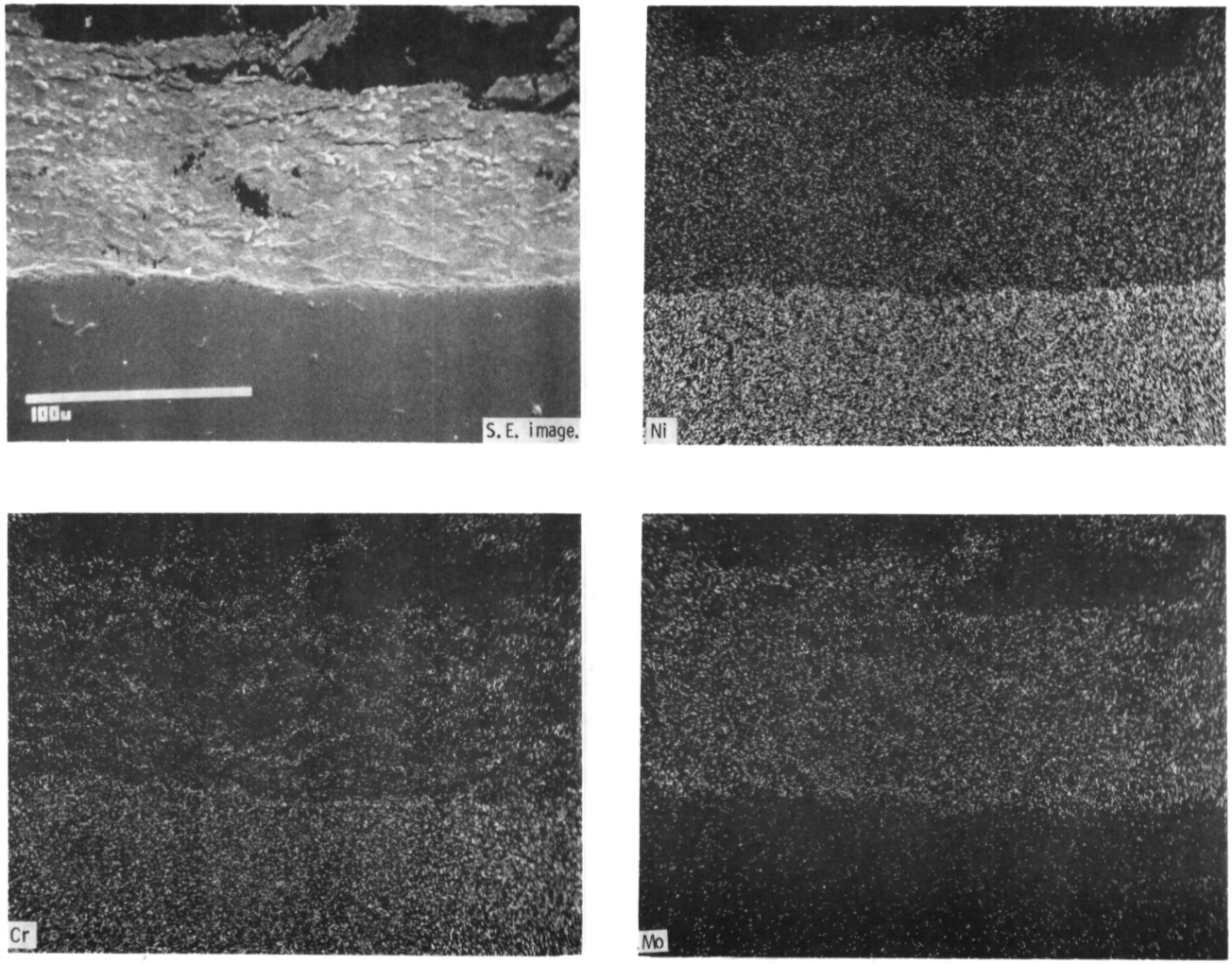

(a) S. E. image and X-ray maps.

Figure 12. - Details of the pit in figure 11.

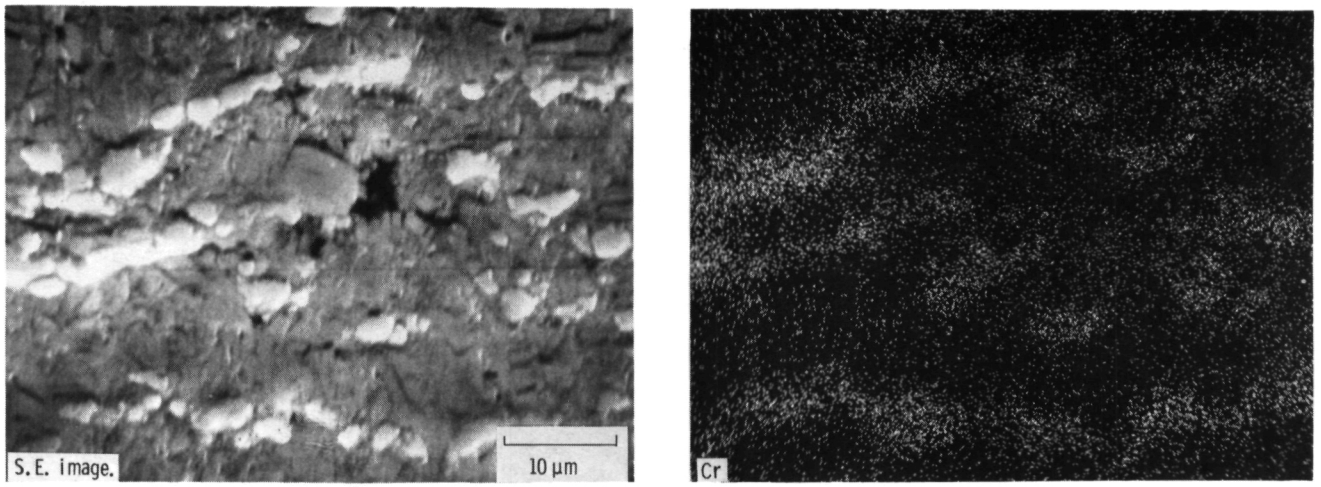

(b) Pit at a higher magnification showing Cr_2O_3 precipitates.

Figure 12. - Concluded.

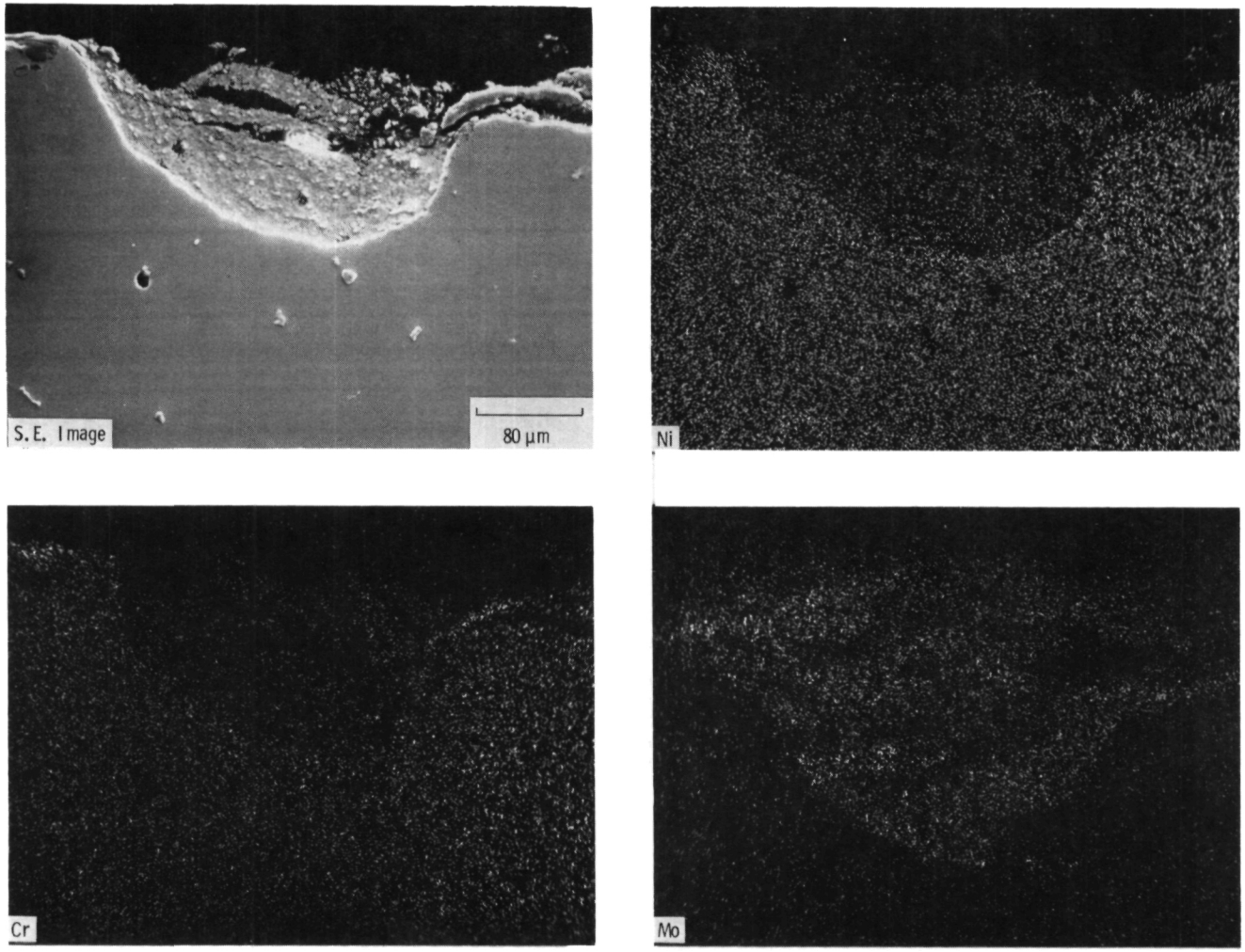

Figure 13. - Scale morphology during the period of catastrophic corrosion for a sample coated with 1.4 mg/cm^2 Na_2MoO_4 and oxidized in 1 atm O_2 for 40 hrs at 950^0 C.

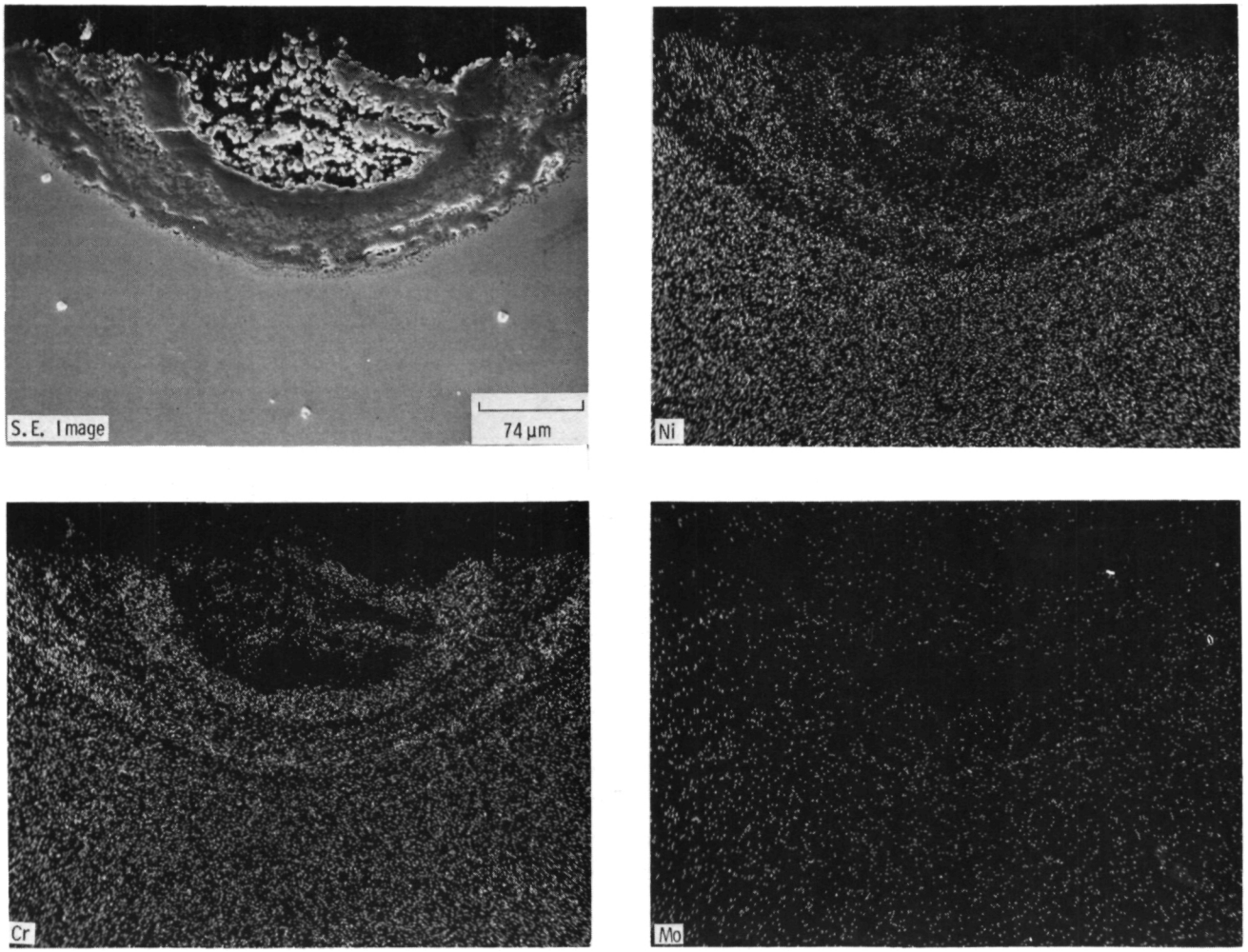

Figure 14. - Scale morphology at the end of the period of catastrophic corrosion for a sample coated with 1.45 mg/cm^2 Na_2MoO_4 and oxidized in 1 atm O_2 for 70 hrs at 950^0 C.

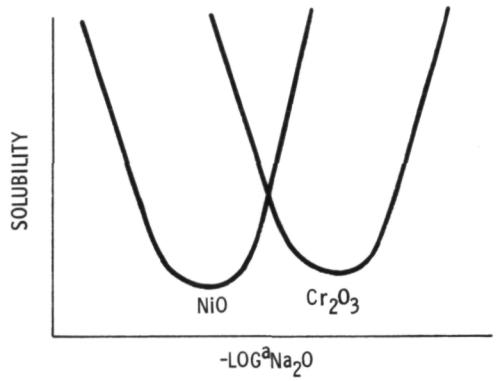

Figure 15. - Schematics of the plot of the solubility of oxides versus - log ^{a} Na_2O.

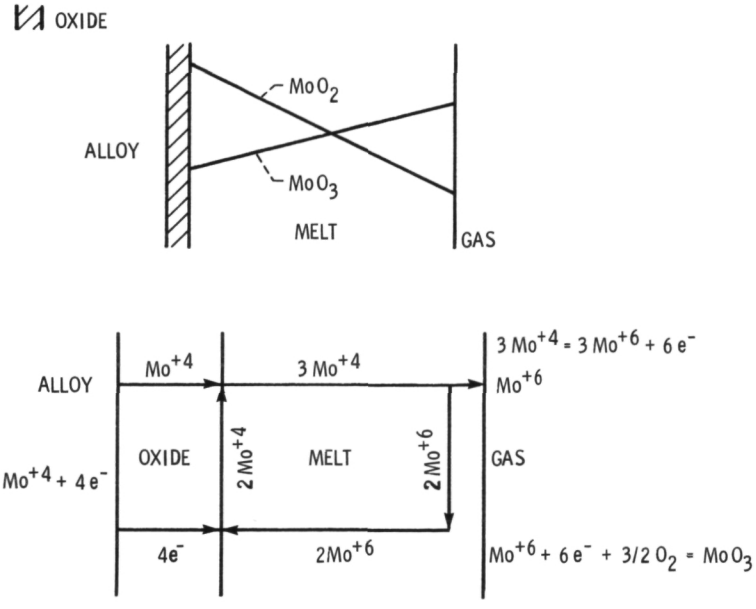

Figure 16. - Schematics of the mechanism of oxidation of Mo beneath the Na_2MoO_4 - MoO_3 melt.

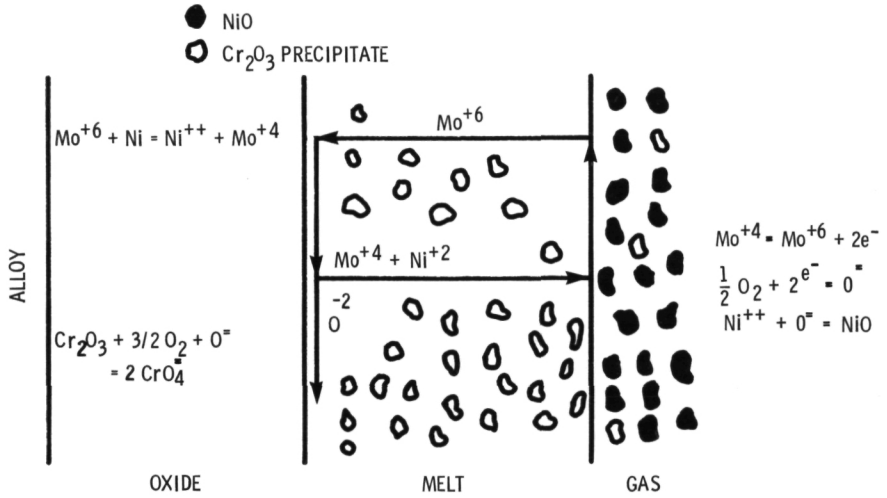

Figure 17. - Schematics of the mechanism of corrosion during the period of catastrophic corrosion.

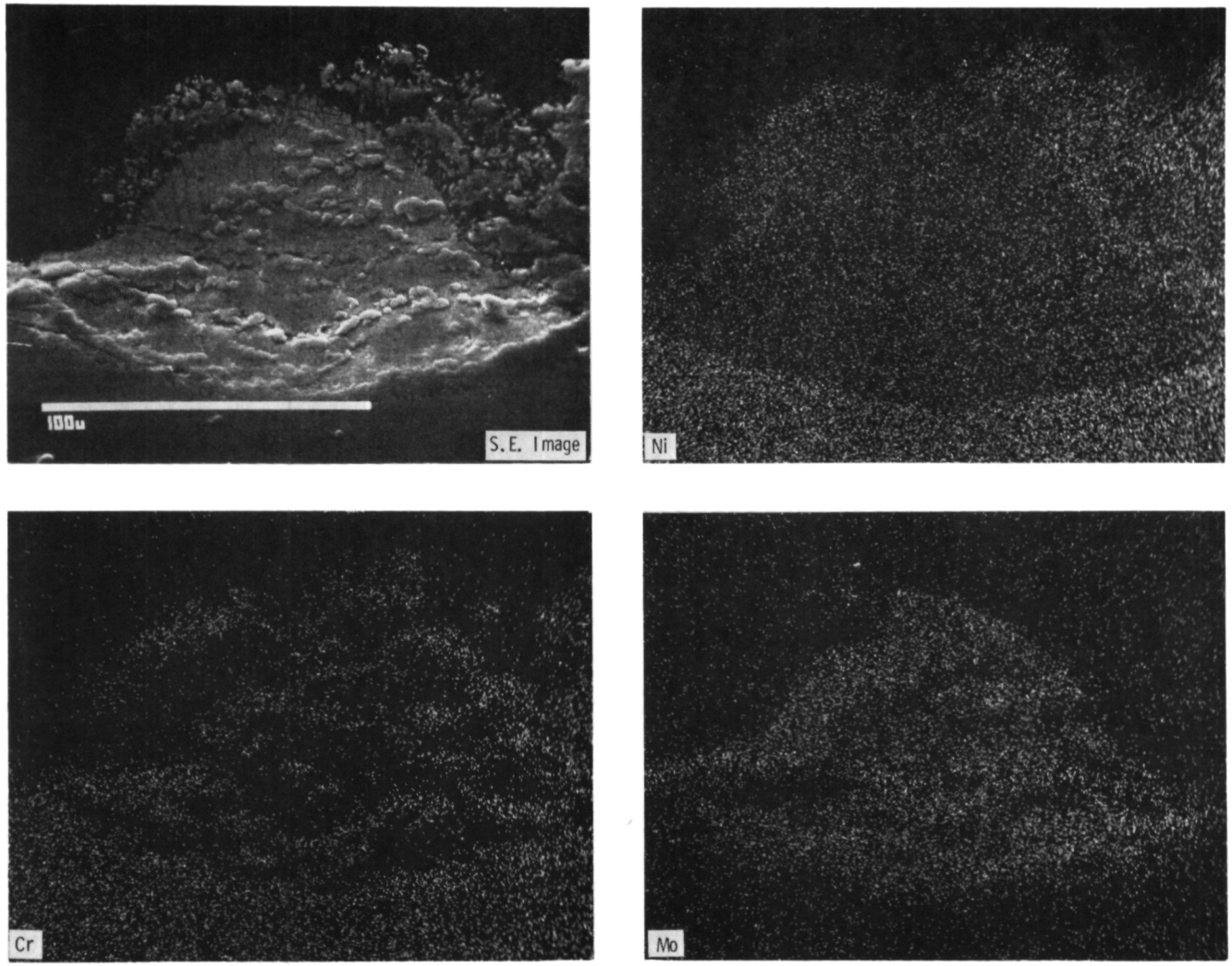

Figure 18. - S. E. image and X-ray maps for U-700, coated with 0.8 mg/cm^2 MoO_3 and oxidized on 1 atm O_2 for 15 hrs at 800^0 C.

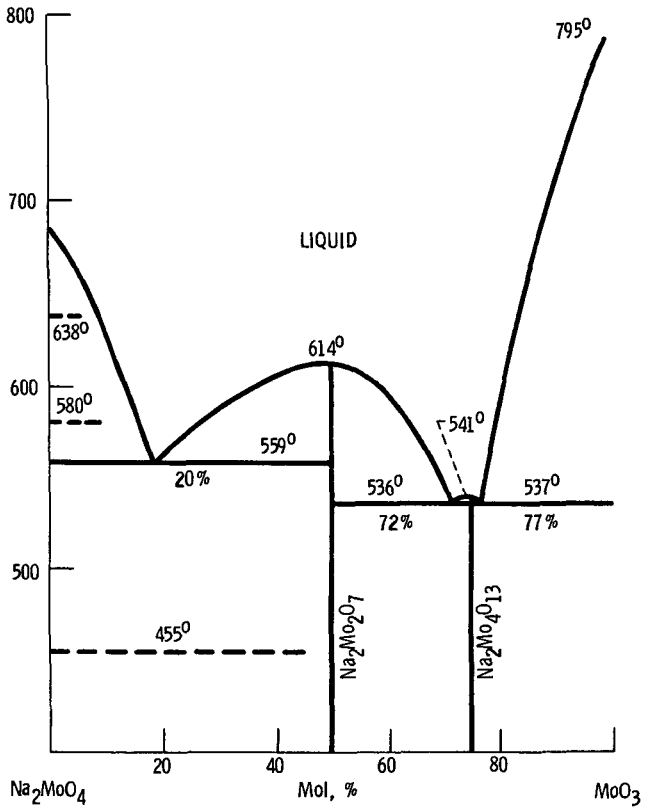

Figure 19. - Na_2MoO_4 - MoO_3 phase diagram.

1. Report No.	2. Government Accession No.	3. Recipient's Catalog No.
NASA TM-83580		

4. Title and Subtitle	5. Report Date
Mechanism of Corrosion of Ni Base Superalloys by Molten Na_2MoO_4 at Elevated Temperatures	
	6. Performing Organization Code: 533-04-1E
7. Author(s): Ajaya K. Misra and Carl A. Stearns	8. Performing Organization Report No: E-1970
	10. Work Unit No
9. Performing Organization Name and Address: National Aeronautics and Space Administration, Lewis Research Center, Cleveland, Ohio 44135	11. Contract or Grant No.
	13. Type of Report and Period Covered: Technical Memorandum
12. Sponsoring Agency Name and Address: National Aeronautics and Space Administration, Washington, D.C. 20546	14. Sponsoring Agency Code

15. Supplementary Notes

Ajaya K. Misra, NRC-NASA Resident Research Associate. Prepared for the Fall Meeting of the Electrochemical Society, Washington, D.C., October 9-14, 1983.

16. Abstract

The corrosion of nickel base superalloy, U-700, by molten Na_2MoO_4 has been studied in the temperature range 750° to 950° C. After an induction period, the rate of corrosion is linear and catastrophic corrosion is observed. The induction period is shown to be associated with the attainment of a minimum MoO_3 activity in the melt, which corresponds to the equilibrium MoO_3 activity for the reaction, $2MoO_3(\ell) + Mo = 3MoO_2(s)$. A mechanism is proposed to describe the catastrophic nature of corrosion, which involves transport of Ni^{++} through the melt resulting in formation of NiO at the melt-gas interface and basic fluxing of Cr_2O_3. The effect of the amount of Na_2MoO_4 on the corrosion kinetics has also been studied. Evaporation studies and the thermodynamic calculations for the Na_2MoO_4 - MoO_3 system have shown that the activity of MoO_3 is reduced considerably when dissolved in Na_2MoO_4, thus causing a sharp decrease in the rate of evaporation of MoO_3 from a Na_2MoO_4 - MoO_3 melt.

17. Key Words (Suggested by Author(s))	18. Distribution Statement
Nickel alloys; Corrosion; Sodium sulfate; Sodium molybdate	Unclassified - unlimited STAR Category 26

19. Security Classif. (of this report)	20. Security Classif. (of this page)	21. No. of pages	22. Price*
Unclassified	Unclassified		

*For sale by the National Technical Information Service, Springfield, Virginia 22161

National Aeronautics and
Space Administration

Washington, D.C.
20546

Official Business
Penalty for Private Use, $300

SPECIAL FOURTH CLASS MAIL
BOOK

Postage and Fees Paid
National Aeronautics and
Space Administration
NASA-451

NASA

POSTMASTER: If Undeliverable (Section 158
Postal Manual) Do Not Return